Karlsruhe Institute of Technology

wave phenomena
analysis and numerics

A microlocal and visual comparison of 2D Kirchhoff migration formulas in seismic imaging

Kevin Ganster, Eric Todd Quinto, Andreas Rieder

CRC Preprint 2024/11, April 2024

KARLSRUHE INSTITUTE OF TECHNOLOGY

CRC 1173

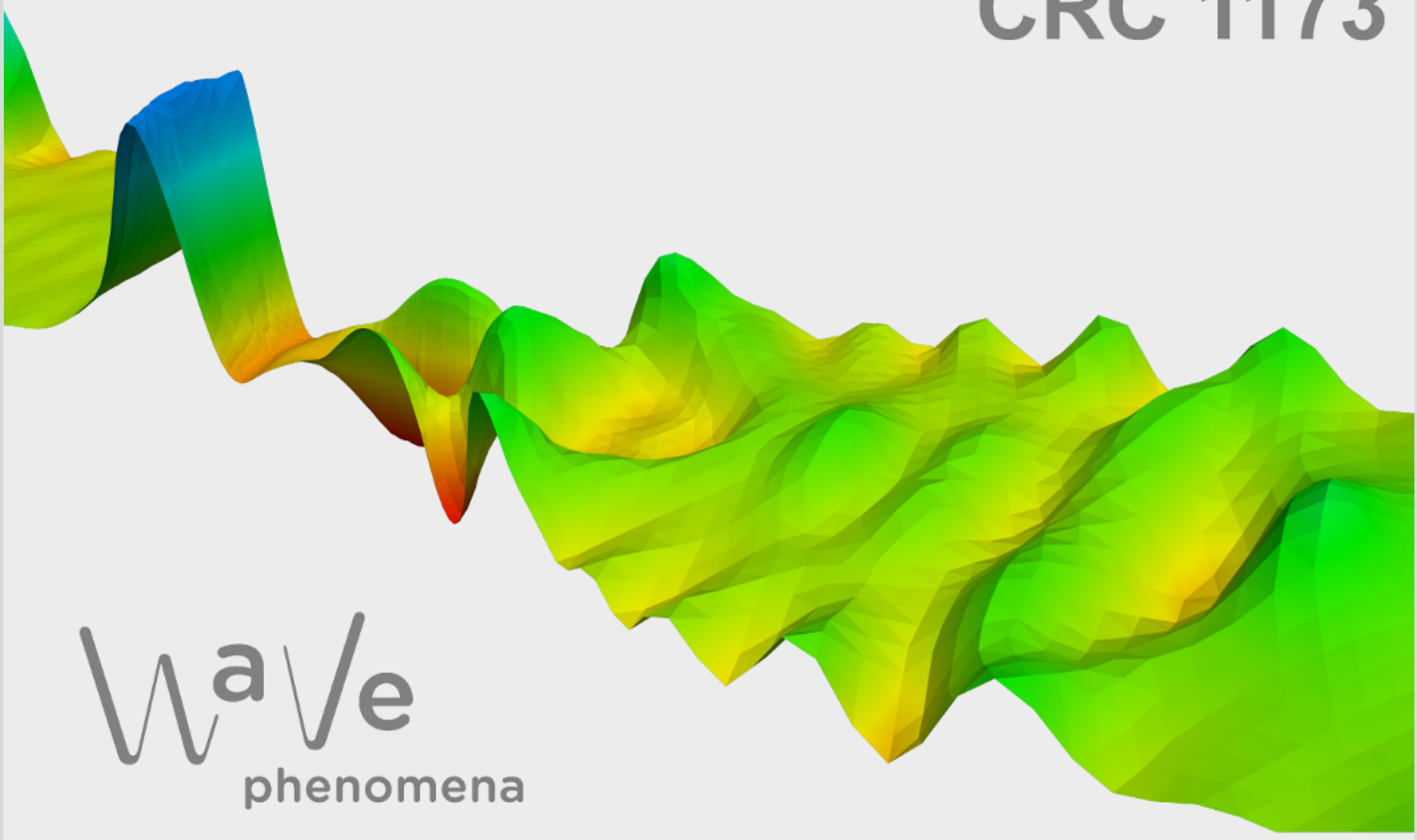

Participating universities

Funded by

ISSN 2365-662X

A MICROLOCAL AND VISUAL COMPARISON OF 2D KIRCHHOFF MIGRATION FORMULAS IN SEISMIC IMAGING

KEVIN GANSTER, ERIC TODD QUINTO, AND ANDREAS RIEDER

ABSTRACT. The term *Kirchhoff migration* refers to a collection of approximate linearized inversion formulas for solving the inverse problem of seismic tomography which entails reconstructing the Earth's subsurface from reflected wave fields. A number of such formulas exists, the first dating from the 1950s. As far as we know, these formulas have not yet been mathematically compared with respect to their imaging properties. This shortcoming is to be alleviated by the present work: we systematically discuss the advantages and disadvantages of the formulas in 2D from a microlocal point of view. To this end we consider the corresponding imaging operators in an unified framework as pseudodifferential or Fourier integral operators. Numerical examples illustrate the theoretical insights and allow a visual comparison of the different formulas.

Dedicated to Alfred K. Louis on the occasion of his 75th birthday.

1. INTRODUCTION

Wave propagation in a medium that does not admit shear stress is accurately modeled by the acoustic wave equation when, in addition, attenuation is neglected: the pressure wave $u = u(t; \boldsymbol{x}, \boldsymbol{x_s})$ at $\boldsymbol{x} = (x_1, x_2)^\top \in \mathbb{R}^2$ and time $t \geq 0$ satisfies

$$\frac{1}{\nu_{\mathrm{p}}^2}\,\partial_t^2 u - \Delta_{\boldsymbol{x}} u = \delta(\boldsymbol{x} - \boldsymbol{x_s})\delta(t), \qquad u|_{t=0} = \partial_t u|_{t=0} = 0, \tag{1}$$

where the wave is initiated by a source at location $\boldsymbol{x_s}$ and time $t = 0$ (δ denotes the Dirac distribution in the related variables and $-\Delta_{\boldsymbol{x}}$ is the Laplacian differential operator in the spatial variables).

The seismic inverse problem in the acoustic regime that we consider reads: reconstruct the sound speed ν_{p} in an open set $X \subset \mathbb{R}^2_+ := \mathbb{R} \times [0, \infty)$ from reflected fields $u(t; \boldsymbol{x_r}, \boldsymbol{x_s})$, $(t; \boldsymbol{x_r}, \boldsymbol{x_s}) \in [0, T] \times \mathfrak{R} \times \mathfrak{S}$. Here $\mathfrak{S}$ and $\mathfrak{R}$ are sets of source and receiver positions in $\partial\mathbb{R}^2_+ = \mathbb{R} \times \{0\}$, respectively, and T is the observation time. The positive x_2-coordinate points downwards into the earth or the ocean.

We linearize this nonlinear inverse problem by

$$\frac{1}{\nu_{\mathrm{p}}^2(\boldsymbol{x})} = \frac{1 + n(\boldsymbol{x})}{v^2(\boldsymbol{x})} \tag{2}$$

with a smooth, a priori known background velocity $v = v(\boldsymbol{x})$ satisfying the geometric optics assumption, that is, any two points in the medium can be connected by a unique ray of geometric

Date: April 18, 2024.

2010 *Mathematics Subject Classification.* 35S30, 45Q05, 65R32, 86A22.

Key words and phrases. Kirchhoff migration, seismic imaging, generalized Radon transform, approximate inverse.

Funded by the Deutsche Forschungsgemeinschaft (DFG, German Research Foundation) - Project-ID 258734477 - SFB 1173. The second author was partially funded by Simons Foundation grant 708556.

optics. Rays are the characteristic curves of the eikonal equation (see (6) below). Hence, multiple reflections are excluded under the geometric optics assumption. The perturbation n in (2) captures the high frequency content of ν_{p} and is the quantity of interest in seismic imaging.

We assume that pairs of source and receiver positions can be smoothly parametrized by a variable s in an open subset $\mathcal{S} \subset \mathbb{R}$, that is, $\boldsymbol{x_r} = \boldsymbol{x_r}(s)$ and $\boldsymbol{x_s} = \boldsymbol{x_s}(s)$. Let $\widetilde{u}$ be the reference solution that has to be computed from (1) with v in place of ν_{p}. Then, using principles of wave propagation under the geometric optics assumption it can be derived that n approximately solves an integral equation, that is,

$$Fn(s,t) \approx 4\pi \int_0^t (u - \widetilde{u})(r; \boldsymbol{x_r}(s), \boldsymbol{x_s}(s))\mathrm{d}r \tag{3}$$

with the operator F being the generalized Radon transform (GRT)

$$Fw(s,t) = \int_X A(s,\boldsymbol{x}) w(\boldsymbol{x}) \delta\big(t - \varphi(s,\boldsymbol{x})\big)\mathrm{d}\boldsymbol{x} \tag{4}$$

where

$$A(s,\boldsymbol{x}) = \frac{a(\boldsymbol{x},\boldsymbol{x_s}(s))a(\boldsymbol{x},\boldsymbol{x_r}(s))}{v^2(\boldsymbol{x})}, \qquad \varphi(s,\boldsymbol{x}) = \tau(\boldsymbol{x},\boldsymbol{x_s}(s)) + \tau(\boldsymbol{x},\boldsymbol{x_r}(s)). \tag{5}$$

The travel time τ and the amplitude a can be computed from

$$|\nabla_{\boldsymbol{x}} \tau(\cdot,\boldsymbol{y})|^2 = v^{-2}(\cdot), \quad \tau(\boldsymbol{y},\boldsymbol{y}) = 0, \tag{6}$$

and

$$\mathrm{div}_{\boldsymbol{x}}\big(a^2(\cdot,\boldsymbol{y})\nabla_{\boldsymbol{x}}\tau(\cdot,\boldsymbol{y})\big) = 0, \quad \lim_{\boldsymbol{x}\to\boldsymbol{y}} a(\boldsymbol{x},\boldsymbol{y})|\boldsymbol{x}-\boldsymbol{y}|^{1/2} = \frac{\sqrt{v(\boldsymbol{y})}}{2\sqrt{2\pi}},$$

see, e.g., [25] and [8]. Note that F is in fact a GRT as it integrates along reflection isochrones

$$\mathcal{L}_{(s,t)} = \{\boldsymbol{x} \in X : t = \varphi(s,\boldsymbol{x})\}. \tag{7}$$

The migration formulas for recovering n from (3), which are known to us and which we investigate here, can be divided into the following two types

$$n \approx F_W^\dagger M g \quad \text{and} \quad n \approx K F_W^\dagger g \tag{8}$$

where M and K are appropriate pseudodifferential operators and $g = g(s,t)$ are the data, for instance, the right hand side of (3). Further, $F_W^\dagger$ denotes the generalized backprojection with weight $W \in \mathcal{C}^\infty(\mathcal{S}\times\Omega)$, that is,

$$F_W^\dagger g(\boldsymbol{x}) = \int_{\mathcal{S}} W(s,\boldsymbol{x}) g(s,\varphi(s,\boldsymbol{x}))\mathrm{d}s.$$

The formal L^2-adjoint F^* has weight $W = A$.

The quality and suitability of these formulas depend on how well the associated imaging operators

$$F_W^\dagger M F \quad \text{and} \quad K F_W^\dagger F \tag{9}$$

emulate the identity operator. For instance, if $F_W^\dagger M F = \mathrm{Id}$ would hold, then we could recover n from consistent data $g = Fn$. To the best of our knowledge neither M nor K are known that will yield the identity. Therefore, we study mapping properties of the different imaging operators to understand which features of n they recover, emphasize or de-emphasize.

Our presentation is organized as follows. Concepts from microlocal analysis are paramount to understand the action of the operators and to describe their subtle differences. The next section therefore introduces those basic parts of the theory that are essential to our subsequent

considerations. In Section 3 we specify in detail the imaging operators we will focus on, that is, we define W, M, and K in (9). In total we investigate four operators: two of the left kind in (9) and two of the right kind. The two of the left kind originate from classical Kirchhoff migration schemes from Geophysics as presented, e.g., in [2]. By our general approach from [8] we compute principal symbols of all operators and study their microlocal properties. In this way, we determine in what respects the operators differ or are similar. For instance, we prove that two of the operators are microlocally close to the identity under the zero-offset scanning geometry and a constant background velocity v, see Corollaries 3.6 and 3.8. Our theoretical findings are illustrated by various numerical examples in Section 5 relying on a numerical scheme from [6] which we briefly summarize in Section 4. We present two sets of reconstructions. For the first set we parameterize source and receiver positions by the common offset scanning geometry and we use consistent data, that is, for a given n we compute numerically $g = Fn$ as input data to our numerical scheme. So we are committing a kind of inverse crime, but it is a venial sin, because it gives us a fairly accurate image of $F_W^\dagger MFn$ and $KF_W^\dagger Fn$, where we can clearly observe the predicted mapping properties of each operator. For the second set of experiments, we generate data by numerically solving the wave equation (1). Moreover, we simulate field data by using the common source scanning geometry for data recording and by allowing only a few sources and receivers, the exact locations of which are randomly perturbed for data generation. In addition, we corrupt the seismograms by artificial random noise. The last Section 6 contains an outline of how the microlocal results of Section 3 carry over to the three-dimensional situation. A rather technical calculation, which does not fit harmoniously into the body of this paper, is presented in an appendix.

2. Microlocal basics

Here, we recall standard facts about Fourier integral and pseudodifferential operators. We collect only what is necessary for our presentation in the following sections and refer to [13, 18, 26, 27] for full details.

Throughout this section, X and Y will be nonempty open subsets of $\mathbb{R}^d$ and $N \in \mathbb{N}$. The definitions are essentially the same if $\dim(X) \neq \dim(Y)$, but we do not need this generality.

We let $\mathbb{N}_0 = \mathbb{N} \cup \{0\}$. If $f\colon X \to \mathbb{R}$, then we define $\nabla_{\boldsymbol{x}} f = \left(\frac{\partial f}{\partial x_1}, \frac{\partial f}{\partial x_2}, \cdots, \frac{\partial f}{\partial x_d}\right)$. If $\alpha = (\alpha_1, \alpha_2, \ldots, \alpha_d) \in \mathbb{N}_0^d$, we use the standard notation for the differential operator D^α by $D^\alpha f = \frac{\partial^{\alpha_1}}{\partial x_1^{\alpha_1}} \frac{\partial^{\alpha_2}}{\partial x_2^{\alpha_2}} \cdots \frac{\partial^{\alpha_d}}{\partial x_d^{\alpha_d}} f$. Finally, $\mathcal{D}(X)$ is the set of all $\mathcal{C}^\infty$ functions of compact support in X, $\mathcal{S}(\mathbb{R}^d)$ is the set of all $\mathcal{C}^\infty$ functions on $\mathbb{R}^d$ that rapidly decrease at infinity along with their derivatives, and $\mathcal{E}(X)$, the set of all $\mathcal{C}^\infty$ functions on X. They are all given their standard topologies [22]. The corresponding dual spaces, $\mathcal{D}'(X)$, the set of distributions on X, $\mathcal{S}'(\mathbb{R}^d)$ the set of tempered distributions on $\mathbb{R}^d$, and $\mathcal{E}'(X)$, which is the set of distributions of compact support on X, are given the appropriate weak topologies.

Some concepts defined below are usually formulated for cotangent bundles. However, because the sets we consider are all subsets of Euclidean space, we will identify each covector $(\boldsymbol{x}, \xi \mathrm{d}\boldsymbol{x}) \in T^*(X)$ by the corresponding vector $(\boldsymbol{x}, \xi) \in X \times \mathbb{R}^d$.

An essential tool is the Fourier transform $\widehat{f} = \mathcal{F}f$ of $f \in L^1(\mathbb{R}^d)$ defined by

$$\widehat{f}(\xi) = \mathcal{F}f(\xi) = \int_{\mathbb{R}^d} f(\boldsymbol{x}) \mathrm{e}^{-\imath \xi \cdot \boldsymbol{x}} \mathrm{d}\boldsymbol{x}, \quad \xi \in \mathbb{R}^d.$$

It is a homeomorphism of $\mathcal{S}(\mathbb{R}^d)$ into $\mathcal{S}(\mathbb{R}^d)$ that can be extended to $\mathcal{S}'(\mathbb{R}^d)$ by duality, see, e.g., [22]. Note that $\mathcal{E}'(X) \subset \mathcal{S}'(\mathbb{R}^d)$.

Our first definition categorizes L^2 smoothness.

Definition 2.1 (Sobolev space [18]). *Let $r \in \mathbb{R}$. The* Sobolev space $H^r(\mathbb{R}^d)$ *is the set of all $u \in \mathcal{S}'(\mathbb{R}^d)$ that have locally integrable Fourier transform $\widehat{u}$ such that*

$$\|u\|_r^2 = \int_{\mathbb{R}^d} |\widehat{u}(\xi)|^2 \left(1 + |\xi|^2\right)^r \, \mathrm{d}\xi$$

is finite.

If K is a compact subset of $\mathbb{R}^d$, then we define $H^r(K)$ to be the subspace of $H^r(\mathbb{R}^d)$ of all distributions supported in K.

For $X \subset \mathbb{R}^d$, we define $H^r_{\text{loc}}(X)$ to be the set of all distributions in $\mathcal{D}'(X)$ such that $\phi u \in H^r(\mathbb{R}^d)$ for every $\phi \in \mathcal{D}(X)$.

Here are some observations about this definition. Note that $\|\cdot\|_r$ is a norm on $H^r(\mathbb{R}^d)$, and $H^r(\mathbb{R}^d)$ is a Hilbert space under this Sobolev norm. If K is a compact subset of $\mathbb{R}^d$, then $H^r(K)$ is a closed subspace of $H^r(\mathbb{R}^d)$ and so is a Hilbert Space. For $\phi \in \mathcal{D}(X)$, $u \mapsto \|\phi u\|_r$ is a seminorm on $H^r_{\text{loc}}(X)$, and the set of all these seminorms topologizes $H^r_{\text{loc}}(X)$ as a Fréchet space. Also, note that if $f \in H^r(\mathbb{R}^d)$ and $r \in \mathbb{N}$, then any partial derivative of f of order less than or equal to r is in $L^2(\mathbb{R}^d)$.

Our next two definitions provide a precise description of singularity. We follow the development in [14, Section 8.1].

Definition 2.2 (Frequency Set). *Let $u \in \mathcal{E}'(\mathbb{R}^d)$, and let V be a cone in $\mathbb{R}^d \backslash \{\mathbf{0}\}$. The Fourier transform $\mathcal{F}u$ is* rapidly decaying on V *if for each $N \in \mathbb{N}$ there is a $C_N > 0$ such that*

$$|\mathcal{F}v(\xi)| \leq C_N(1 + |\xi|)^{-N}, \ \textit{for all} \ \xi \in V.$$

The frequency set of u, $\Sigma(u)$, *is the cone of all $\eta \in \mathbb{R}^d \backslash \{\mathbf{0}\}$ having no conic open neighborhood V such that $\mathcal{F}u$ is rapidly decaying in V.*

For each $\boldsymbol{x} \in \mathbb{R}^d$, define

$$\Sigma_{\boldsymbol{x}}(u) = \bigcap_{\phi \in \mathcal{D}(X),\ \phi(\boldsymbol{x}) \neq 0} \Sigma(\phi u).$$

Since the complement of $\Sigma(u)$ is open, $\Sigma(u)$ is a closed set, and $u \in \mathcal{D}(\mathbb{R}^d)$ if and only if $\Sigma(u) = \emptyset$. By the definition of $\Sigma(u)$, the Fourier transform $\mathcal{F}u$ is rapidly decaying at ∞ in every closed conic subset of the complement of $\Sigma(u)$. The set $\Sigma_{\boldsymbol{x}}(u)$ represents the set of directions at which u is not smooth at $\boldsymbol{x}$, and this is the key idea in the following definition.

Definition 2.3 (Wave front set). *Let $X \subset \mathbb{R}^d$ be open and let $u \in \mathcal{D}'(X)$.*

The wave front set $\mathrm{WF}(u)$ *of u is the set*

$$\mathrm{WF}(u) = \left\{(\boldsymbol{x}, \xi) \in X \times (\mathbb{R}^d \backslash \{\mathbf{0}\}) : \ \xi \in \Sigma_{\boldsymbol{x}}(u)\right\}.$$

Note that $\Sigma(u)$ is the projection of $\mathrm{WF}(u)$ onto the second (cotangent) coordinate [14, Proposition 8.1.3].

2.1. **Fourier integral operators.** Fourier integral operators (FIO) are defined in terms of phase functions and symbols, and we start by giving these terms. Let X and Y be open subsets of $\mathbb{R}^d$. Our definitions and theorems hold when X and Y have different dimensions, but our applications do not need this.

Definition 2.4 (Phase function). *A real-valued function $\Phi \in \mathcal{E}(Y \times X \times \mathbb{R}^N \backslash \{\mathbf{0}\})$ with arguments $(\boldsymbol{y}, \boldsymbol{x}, \xi)$ is called a* phase function *if it is positively homogeneous of degree 1 in ξ and $(\nabla_{\boldsymbol{y}}\Phi, \nabla_\xi \Phi)$ as well as $(\nabla_{\boldsymbol{x}}\Phi, \nabla_\xi \Phi)$ do not vanish on $Y \times X \times \mathbb{R}^N \backslash \{\mathbf{0}\}$.*

The phase function is nondegenerate *if the set* $\{\nabla_{(\boldsymbol{y},\boldsymbol{x},\xi)}\partial_{\xi_j}\Phi : j = 1,\dots,N\}$ *is linearly independent on the manifold*

$$\Sigma_\Phi = \{(\boldsymbol{y},\boldsymbol{x},\xi) \in Y \times X \times \mathbb{R}^N \backslash \{\mathbf{0}\} : \nabla_\xi \Phi(\boldsymbol{y},\boldsymbol{x},\xi) = 0\}.$$

Definition 2.5 (Standard Symbol)**.** *A function* $p \in \mathcal{E}(Y \times X \times \mathbb{R}^N)$ *is a* standard symbol *(or standard full symbol) of order* $m \in \mathbb{R}$ *if for every compact set* $\mathrm{K} \subset Y \times X$ *and all multi-indices* $\alpha \in \mathbb{N}_0^N$, $\beta \in \mathbb{N}_0^d$, *and* $\gamma \in \mathbb{N}_0^d$ *there exists a positive constant* $C = C(\mathrm{K},\alpha,\beta,\gamma)$ *such that*

$$|D_\xi^\alpha D_{\boldsymbol{x}}^\beta D_{\boldsymbol{y}}^\gamma p(\boldsymbol{y},\boldsymbol{x},\xi)| \leq C(1+|\xi|)^{m-|\alpha|}$$

holds for all $(\boldsymbol{y},\boldsymbol{x}) \in \mathrm{K}$ *and all* ξ *with* $|\xi| \geq 1$. *The set of all symbols of order* m *is denoted by* $S^m(Y \times X \times \mathbb{R}^N)$.

If $p \in S^m(Y \times X \times \mathbb{R}^N)$, *then* p *is* elliptic of order m *(or elliptic if the order is clear) if, for each compact subset* K *of* $Y \times X$, *there are positive constants* c *and* M *such that*

$$|p(\boldsymbol{y},\boldsymbol{x},\xi)| \geq c\,(1+|\xi|)^m$$

for all $(\boldsymbol{y},\boldsymbol{x}) \in \mathrm{K}$ *and all* ξ *with* $|\xi| \geq M$.

Definition 2.6 (Fourier Integral Operator)**.** *Given a standard symbol* $p \in S^m(Y \times X \times \mathbb{R}^N)$ *and a nondegenerate phase function* $\Phi \in \mathcal{E}(Y \times X \times \mathbb{R}^N \backslash \{\mathbf{0}\})$ *we define the* Fourier integral operator *(FIO)* F *applied to* $u \in \mathcal{D}(X)$ *by*

$$Fu(\boldsymbol{y}) = \int_{\mathbb{R}^N} \int_X p(\boldsymbol{y},\boldsymbol{x},\xi) u(\boldsymbol{x}) \mathrm{e}^{\imath\Phi(\boldsymbol{y},\boldsymbol{x},\xi)}\,\mathrm{d}\boldsymbol{x}\,\mathrm{d}\xi. \tag{10}$$

The order *of the operator* F *is* $k := m - \left(\frac{d-N}{2}\right)$.

If F is an FIO then (10) is an oscillatory integral and F maps $\mathcal{D}(X)$ continuously to $\mathcal{E}(Y)$ and can be extended as a continuous map from $\mathcal{E}'(X)$ to $\mathcal{D}'(Y)$, see [13, Chap. I].

Definition 2.7 (Canonical Relation)**.** *If* F *is an FIO with phase function* $\Phi \in \mathcal{E}(Y \times X \times \mathbb{R}^N \backslash \{\mathbf{0}\})$, *then the* canonical relation of F *is the set*

$$C = \left\{\left(\boldsymbol{y}, \nabla_{\boldsymbol{y}}\Phi(\boldsymbol{y},\boldsymbol{x},\xi); \boldsymbol{x}, -\nabla_{\boldsymbol{x}}\Phi(\boldsymbol{y},\boldsymbol{x},\xi)\right) : (\boldsymbol{y},\boldsymbol{x},\xi) \in \Sigma_\Phi\right\} \subset T^*(Y) \times T^*(X).$$

The canonical relation, C, of an FIO encodes how the FIO propagates singularities:

$$\mathrm{WF}(Fu) \subset C \circ \mathrm{WF}(u), \tag{11}$$

by the Hörmander-Sato Lemma [14, Theorem 8.2.12]. We denote the canonical left projection from C to $T^*(Y)$ by $\Pi_\mathrm{L} \colon C \to T^*(Y)$ and the canonical right projection by $\Pi_\mathrm{R} \colon C \to T^*(X)$.

Definition 2.8 (The Bolker Condition [10, 11])**.** *Let* $F \colon \mathcal{E}'(X) \to \mathcal{D}'(Y)$ *be an FIO and let* C *be its canonical relation. Then* F *(or* C*) satisfies the* Bolker condition *if*

$$\Pi_\mathrm{L} \colon C \to T^*(Y) \text{ is an injective immersion.}$$

If an FIO F satisfies the Bolker condition, then it has important microlocal properties. Let F^* be the formal L^2 adjoint of F. Assume that F^*F is well defined. Then, under the Bolker condition, F^*F is a pseudodifferential operator, see [11]. Pseudodifferential operators are introduced in the next subsection, and they are FIOs with favorable qualities for imaging, which we exploit in Section 3.

2.2. **Pseudodifferential Operators.** Pseudodifferential operators are FIOs where $X = Y \subset \mathbb{R}^d$ and $\Phi(\boldsymbol{y}, \boldsymbol{x}, \xi) = (\boldsymbol{y} - \boldsymbol{x}) \cdot \xi$ is the nondegenerate phase function.

In the applications we consider in the next sections, the symbols of the pseudodifferential operators depend only on the two variables $\boldsymbol{x}$ and ξ. All concepts and results of the previous subsection carry over. Since $\xi \in \mathbb{R}^d$ we write $S^m(X)$ instead of $S^m(X \times \mathbb{R}^d)$.

Hence, for $p \in S^m(X)$, the linear map $P\colon \mathcal{E}'(X) \to \mathcal{D}'(X)$,

$$Pu(\boldsymbol{x}) = \int_{\mathbb{R}^d} \int_X p(\boldsymbol{x}, \xi) u(\boldsymbol{y}) \mathrm{e}^{\imath(\boldsymbol{x}-\boldsymbol{y})\cdot\xi} \, \mathrm{d}\boldsymbol{y} \, \mathrm{d}\xi = \int_{\mathbb{R}^d} p(\boldsymbol{x}, \xi) \widehat{u}(\xi) \mathrm{e}^{\imath \boldsymbol{x}\cdot\xi} \, \mathrm{d}\xi \tag{12}$$

is a *standard pseudodifferential operator* (ΨDO) of order m. Here, p is called the *full symbol* of the operator P.

A *smoothing operator* is any linear operator that maps $\mathcal{E}'(X)$ continuously into $\mathcal{E}(X)$.

Since ΨDOs are FIOs with specific phase functions, one might expect the symbol p in (12) to be a function of $(\boldsymbol{x}, \boldsymbol{y}, \xi)$ as in Definition 2.6. However, ΨDOs with symbol $p(\boldsymbol{x}, \xi)$ generate the same class of operators modulo smoothing operators as those with symbol $p(\boldsymbol{y}, \boldsymbol{x}, \xi)$ [18, Theorem 4.5, p. 188].

We will study ΨDO with more general symbols and we now give the definition (see [15]).

Definition 2.9 (General Symbol)**.** *Let $p(\boldsymbol{x}, \xi) \in \mathcal{E}(X \times (\mathbb{R}^d \backslash \{\mathbf{0}\}))$ and let $m \in \mathbb{R}$. Then, p is a* general (full) symbol of order m, *$p \in S^m_g(X)$ if the following two conditions hold.*

1. *For every compact set $\mathrm{K} \subset X$ and all multi-indices α and β in $\mathbb{N}_0^d$ there exists a positive constant $C = C(\mathrm{K}, \alpha, \beta)$ such that*
$$|D_\xi^\alpha D_{\boldsymbol{x}}^\beta p(\boldsymbol{x}, \xi)| \leq C(1 + |\xi|)^{m-|\alpha|}$$
holds for all $\boldsymbol{x} \in \mathrm{K}$ and all ξ with $|\xi| \geq 1$.
2. *For all multi-indices $\beta \in \mathbb{N}_0^d$, $D_{\boldsymbol{x}}^\beta p(\boldsymbol{x}, \xi)$ is integrable on $\mathrm{K} \times B$ where B is the unit ball.*

The symbol p is elliptic *if for each compact subset K of X, there are positive constants c and M such that*
$$|p(\boldsymbol{x}, \xi)| \geq c\,(1 + |\xi|)^m$$
for all $\boldsymbol{x} \in \mathrm{K}$ and $|\xi| > M$.

If P is an operator given by (12) with general symbol p then P is a ΨDO [15].

Definition 2.10 (General ΨDO and Principal Symbol)**.** *Let P be a ΨDO given by (12) with general symbol $p \in S^m_g(X)$. The operator P is* elliptic *if its full symbol p is elliptic.*

The (General) Principal Symbol *of P, $\sigma(P)$, is the equivalence class of p in the quotient space $S^m_g(X)/S^{m-1}_g(X)$.*

If P' is a ΨDO with symbol in $S^m_g(X)$, and the linear transformation $P\colon \mathcal{E}'(X) \to \mathcal{D}'(X)$ differs from P' by a smoothing operator, then P will be called a general ΨDO and its general principal symbol will be $\sigma(P')$.

Note that any operator with a standard or general symbol is also a general ΨDO. If P is a general ΨDO, then P differs from a standard ΨDO by a smoothing operator. This is proven using the integrability condition in the definition of general symbol.

Example 2.11. *Let R be the classical Radon transform in $\mathbb{R}^2$ which integrates along straight lines uniquely parameterized by the parallel scanning geometry. Then R^*R is a general ΨDO with full symbol*

$$p(\boldsymbol{x}, \xi) = |\xi|^{-1}, \tag{13}$$

see [15, Theorem 13]*, and a quick exercise shows its symbol is in* $S_g^{-1}(\mathbb{R}^2)$*. Thus,* R^*R *is a general* Ψ*DO that is elliptic of order* -1*.*

Pseudodifferential operators do not create singularities:

$$\mathrm{WF}(Pu) \subset \mathrm{WF}(u) \quad \text{for any } u \in \mathcal{E}'(X). \tag{14}$$

In case P is elliptic (i.e., its symbol is elliptic), equality holds [18, p. 226]:

$$\mathrm{WF}(Pu) = \mathrm{WF}(u) \quad \text{for any } u \in \mathcal{E}'(X). \tag{15}$$

These operators have good continuity properties.

Theorem 2.12. *If* P *is a* Ψ*DO of order* m *on* X *and* K *is a compact subset of* X*, then for every* $r \in \mathbb{R}$*,* P *is a continuous map from* $H^r(K)$ *to* $H^{r-m}_{\mathrm{loc}}(X)$*.*

Proof. In [18, Corollary 3.4, p. 240], it is shown that if P is a ΨDO on X and ϕ and ψ are in $\mathcal{D}(X)$, then the operator $P' = \phi P \psi$ is continuous from $H^r(\mathbb{R}^d)$ to $H^{r-m}(\mathbb{R}^d)$. Therefore the operator $P\psi$ is continuous from $H^r(\mathbb{R}^d)$ to $H^{r-m}_{\mathrm{loc}}(X)$.

Since K is a compact subset of X, there is a function $\psi \in \mathcal{D}(X)$ that is equal to one on a neighborhood of K. Thus, using this ψ, one sees that P is continuous from $H^r(K)$ to $H^{r-m}_{\mathrm{loc}}(X)$. □

Theorem 2.12, (14), and (15) are generally proven for standard ΨDO, but they are true for general ΨDOs since smoothing operators map distributions continuously to $\mathcal{E}(X)$ and do not create singularities. The above theorem holds even for FIOs of order m, see, e.g., [27, Chapter VIII, Theorem 6.1].

3. Imaging operators

3.1. **General setting.** Let $\mathcal{S}$ be an open subset of $\mathbb{R}$, let $\varphi\colon \mathcal{S} \times \mathbb{R}^2_+ \to \mathbb{R}$, and define

$$\mathcal{X} = \mathrm{int}\{\boldsymbol{x} \in \mathbb{R}^2_+ : \forall s \in \mathcal{S} : \nabla_{\boldsymbol{x}} \varphi(s, \boldsymbol{x}) \neq \mathbf{0}\} \quad \text{and} \quad \mathcal{Y} = \{(s,t) : s \in \mathcal{S},\, t > t_{\text{first}}(s)\}$$

where $t_{\text{first}}(s)$ is the time which the unique ray needs from source $\boldsymbol{x_s}(s)$ to receiver $\boldsymbol{x_r}(s)$. Let X be an open connected set with $X \Subset \mathcal{X}$.[1] Let S be an open and connected set with $S \Subset \mathcal{S}$. Define

$$Y = \{(s,t) :\ s \in S,\, t > t_{\text{first}}(s)\} \quad \overline{Y} = \{(s,t) :\ s \in \mathrm{Cl}(S),\, t > t_{\text{first}}(s)\}\,.$$

We now outline why the GRT $F\colon \mathcal{E}'(\mathcal{X}) \to \mathcal{D}'(\mathcal{Y})$ from (4) as well as the generalized backprojection $F^\dagger_W$ are Fourier integral operators of order $-1/2$. These standard arguments are similar to those in, e.g., [8] and [16, equation (3.6)].

By using the Fourier expression for the delta function in (4), we see that

$$Fw(s,t) = \int_{\mathcal{X}} \int_{\mathbb{R}} A(s, \boldsymbol{x}) w(\boldsymbol{x}) \mathrm{e}^{\imath \Phi(s,t,\boldsymbol{x},\omega)}\, \mathrm{d}\omega \mathrm{d}\boldsymbol{x} \tag{16}$$

where

$$\Phi(s,t,\boldsymbol{x},\omega) = \omega(t - \varphi(s,\boldsymbol{x})).$$

Since $t = \varphi(s,\boldsymbol{x})$ when $\Phi(s,t,\boldsymbol{x},\omega) = 0$, we have global coordinates $(s,\boldsymbol{x},\omega)$ on the canonical relation:

$$\begin{gathered} \mathcal{C} = \{(s, \varphi(s,\boldsymbol{x}), -\omega\partial_s\varphi(s,\boldsymbol{x}), \omega; \boldsymbol{x}, \omega\nabla_{\boldsymbol{x}}\varphi(s,\boldsymbol{x})) \ :\ s \in \mathcal{S}, \boldsymbol{x} \in \mathcal{X}, \omega \neq 0\}\,, \\ \mathcal{S} \times \mathcal{X} \times (\mathbb{R}\backslash\{0\}) \ni (s,\boldsymbol{x},\omega) \mapsto (s, \varphi(s,\boldsymbol{x}), -\omega\partial_s\varphi(s,\boldsymbol{x}), \omega; \boldsymbol{x}, \omega\nabla_{\boldsymbol{x}}\Phi)\,. \end{gathered} \tag{17}$$

[1] $A \Subset B$ if $\mathrm{Cl}(A)$ is a compact subset of B.

Recall that we will identify cotangent vectors with their coordinates, e.g., each covector in $T^*(X)$ will be identified with the corresponding point in $X \times \mathbb{R}^2$ in our proofs.

We let

$$
\begin{aligned}
C &= \mathcal{C} \cap \big(Y \times (\mathbb{R}^2 \backslash \{\mathbf{0}\})\big) \times \big(X \times (\mathbb{R}^2 \backslash \{\mathbf{0}\})\big)\,, \\
\overline{C} &= \mathcal{C} \cap \big(\overline{Y} \times (\mathbb{R}^2 \backslash \{\mathbf{0}\})\big) \times \big(\mathrm{Cl}(X) \times (\mathbb{R}^2 \backslash \{\mathbf{0}\})\big)\,.
\end{aligned} \tag{18}
$$

Since $\omega \neq 0$ and $\nabla_{\boldsymbol{x}}\Phi$ is never zero by choice of $\mathcal{X}$, Φ is a nondegenerate phase function. Since the symbol does not have ω dependence, it is of order zero, so the operator $F\colon \mathcal{E}'(\mathcal{X}) \to \mathcal{D}'(\mathcal{Y})$ is an FIO of order $-1/2 = 0 + (1-2)/2$. The analogous argument or [13, Theorem 4.2.1] shows that $F^\dagger$ given by (8) is an FIO associated to the transpose, $\mathcal{C}^\top$, of $\mathcal{C}$.[2]

To calculate the symbol of our imaging operators below, we need to know that there is only a finite number of preimages of any $(\boldsymbol{x}, \xi) \in T^*(X)$ under $\Pi_{\mathrm{R}}\colon C \to T^*(X)$. The set of preimages is finite for many standard transforms, including our GRT F for constant or affine-linear velocity as well as for numerous other Radon transforms. However, in general, this set could be infinite. Our next proposition shows that assuming $S \Subset \mathcal{S}$ takes care of this subtlety.

Lemma 3.1. *Assume that the GRT $F\colon \mathcal{E}'(\mathcal{X}) \to \mathcal{D}'(\mathcal{Y})$ given by (16) satisfies the Bolker condition. Let $(\boldsymbol{x}, \xi) \in \Pi_{\mathrm{R}}(\overline{C})$. Then, there are only a finite number of points in*

$$
\mathcal{I}(\boldsymbol{x}, \xi) = \big\{(s, \omega) \in \mathrm{Cl}(S) \times (\mathbb{R}\backslash\{0\}) : \xi = \omega \nabla_{\boldsymbol{x}} \varphi(s, \boldsymbol{x})\big\}. \tag{19}
$$

This lemma is valid for any canonical relation satisfying the Bolker condition.

Proof of Lemma 3.1. We use coordinates (17) on $\mathcal{C}$ and note

$$
\Pi_{\mathrm{R}}\colon \mathcal{C} \to T^*(X)\backslash\{\mathbf{0}\}, \quad (s, \omega, \boldsymbol{x}) \mapsto \big(\boldsymbol{x}, \omega \nabla_{\boldsymbol{x}} \varphi(s, \boldsymbol{x})\big).
$$

Under the hypotheses of the theorem, the Jacobian matrix $D\Pi_{\mathrm{L}}$ is invertible on $\mathcal{C}$, so $D\Pi_{\mathrm{R}}$ is also invertible and $\Pi_{\mathrm{R}}\colon \mathcal{C} \to T^*(\mathcal{X})\backslash\{\mathbf{0}\}$ is a local diffeomorphism by the Inverse Function Theorem.

Let $(\boldsymbol{x}, \xi) \in \Pi_{\mathrm{R}}(\overline{C})$ and let $I = \Pi_{\mathrm{R}}^{-1}(\boldsymbol{x}, \xi)$ be the set of preimages of $(\boldsymbol{x}, \xi)$ in $\overline{C}$. Since Π_{R} is a local diffeomorphism on $\mathcal{C}$, I is a set of isolated points.

We prove I is finite by contradiction. Assume I is infinite. Then, there are distinct points (s_j, ω_j) for $j \in \mathbb{N}$ such that

$$
\Pi_{\mathrm{R}}(s_j, \varphi(s_j, \boldsymbol{x}), \omega_j \partial_s \varphi(s_j, \boldsymbol{x}), \omega_j; \boldsymbol{x}, \omega_j \nabla_{\boldsymbol{x}} \varphi(s_j, \boldsymbol{x})) = (\boldsymbol{x}, \xi).
$$

If I is bounded, then there is an $(s_0, \omega_0) \in \mathrm{Cl}(S) \times \mathbb{R}$ such that

$$
\lambda = (s_0, \varphi(s_0, \boldsymbol{x}), -\omega_0 \partial_s \varphi(s_0, \boldsymbol{x}), \omega_0; \boldsymbol{x}, \omega_0 \nabla_{\boldsymbol{x}} \varphi(s_0, \boldsymbol{x}))
$$

is an accumulation point of I. By continuity of Π_{R}, $\Pi_{\mathrm{R}}(\lambda) = (\boldsymbol{x}, \xi)$. Since the preimages of $(\boldsymbol{x}, \xi)$ in $\mathcal{C}$ are isolated, I must be unbounded. Therefore, since $\mathrm{Cl}(S)$ is a compact subset of $\mathcal{S}$, the set $\{\omega_j\}$ must be unbounded.

By the definition of $\mathcal{X}$, $\nabla_{\boldsymbol{x}} \varphi(s, \boldsymbol{x}) \neq \mathbf{0}$ for $(s, \boldsymbol{x}) \in \mathcal{S} \times \mathcal{X}$. Since $\mathrm{Cl}(S)$ is a compact subset of $\mathcal{S}$ and $X \Subset \mathcal{X}$, $\nabla_{\boldsymbol{x}} \varphi(s, \boldsymbol{x})$ is bounded away from zero for $(s, \boldsymbol{x}) \in \mathrm{Cl}(S) \times X$. However, for all j, $\omega_j \nabla_{\boldsymbol{x}} \varphi(s_j, \boldsymbol{x}) = \xi$. This is impossible since the set $\{\omega_j\}$ is unbounded. This contradiction proves that I is bounded. Therefore, $\Pi_{\mathrm{L}}(I) = \mathcal{I}(\boldsymbol{x}, \xi)$ is a finite set. □

Our next theorem gives the symbol of our operators for the general setting (9).

[2] $\mathcal{C}^\top$ is $\mathcal{C}$ with the $T^*(\mathcal{X})$ and $T^*(\mathcal{Y})$ coordinates switched.

Theorem 3.2. *Let X and S be open sets, $X \Subset \mathcal{X}$ and $S \Subset \mathcal{S}$ and let C be given by (18). Let F be given by (16) and assume $F\colon \mathcal{E}'(\mathcal{X}) \to \mathcal{D}'(\mathcal{Y})$ satisfies the Bolker condition. Let K be a properly supported general ΨDO on $\mathbb{R}^2$ with symbol $k = k(\boldsymbol{x}, \xi)$ and let L be a general ΨDO on $\mathbb{R}$ with symbol $\ell = \ell(\omega)$. Let $\psi \in \mathcal{D}(S)$. Then, the operator*

$$\mathcal{L} = \frac{1}{2\pi} F_W^\dagger (\mathrm{Id} \otimes L)\, \psi\, F$$

is a well-defined general ΨDO from $\mathcal{E}'(X)$ to $\mathcal{D}'(X)$, as is the operator $K\mathcal{L}$. The principal symbol of $K\mathcal{L}$ is

$$\sigma(K\mathcal{L})(\boldsymbol{x}, \xi) = k(\boldsymbol{x}, \xi) \sum_{(s,\omega)\in \mathcal{I}(\boldsymbol{x},\xi)} \frac{\psi(s) W(s, \boldsymbol{x}) \ell(\omega) A(s, \boldsymbol{x})}{|\omega B(s, \boldsymbol{x})|} \tag{20}$$

where $\mathcal{I}(\boldsymbol{x}, \xi)$ is given by (19) and

$$B(s, \boldsymbol{x}) = \det \begin{pmatrix} \nabla_{\boldsymbol{x}} \varphi(s, \boldsymbol{x}) \\ \partial_s \nabla_{\boldsymbol{x}} \varphi(s, \boldsymbol{x}) \end{pmatrix}.$$

We emphasize that the cutoff function ψ is a technical crutch needed in general so that $F_W^\dagger(\mathrm{Id} \otimes L)$ and ψF can be composed. Without it, the operator $\mathcal{L}$ from the lemma above might not be defined.

The sum in (20) requires some explanation. If $\mathcal{I}(\boldsymbol{x}, \xi_0) = \emptyset$ then we define the sum to be equal to zero. For other points, the sum is finite by Lemma 3.1.

Proof of Theorem 3.2. Since $\sigma(K\mathcal{L}) = k\sigma(\mathcal{L})$ we show $\mathcal{L}$ is well-defined and calculate its symbol as a general ΨDO.

First we show that $\mathcal{L}$ maps from $\mathcal{E}'(X)$ to $\mathcal{D}'(X)$. Since $\mathrm{Cl}(X \times S)$ is a compact subset of $\mathcal{X} \times \mathcal{S}$, the image $\varphi(S, X)$ is a bounded set, $T \subset \mathbb{R}$. Because F integrates $f \in \mathcal{E}'(X)$ over manifolds $t = \varphi(s, \boldsymbol{x})$, $\psi(s) F f(s, t)$ is supported in the compact subset $\mathrm{Cl}(S \times T)$. Therefore $\psi F f$ has compact support. The discussion around (25) below explains why $(\mathrm{Id} \otimes L)\psi F f \in \mathcal{D}'(Y)$ is defined for $f \in \mathcal{E}'(X)$.

Conveniently, because ψ is independent of t,

$$\psi(s)(\mathrm{Id} \otimes L) F f = (\mathrm{Id} \otimes L)\psi(s) F f. \tag{21}$$

For $f \in \mathcal{E}'(X)$, $F_W^\dagger$ integrates $\psi(\mathrm{Id} \otimes L) F f$ over some subset of $\mathrm{Cl}(S \times T)$, which is a compact set. Therefore, $F_W^\dagger \psi(\mathrm{Id} \otimes L) F f(\boldsymbol{x})$ is well defined for $\boldsymbol{x} \in X$.

Note that $\mathrm{Id} \otimes L$ has full symbol

$$\sigma(\mathrm{Id} \otimes L)(s, t, \tau, \omega) = \ell(\omega) \tag{22}$$

in the sense that $\mathrm{Id} \otimes L$ is given by (12) with $p(s, t, \tau, \omega) = \ell(\omega)$. Unless ℓ is smooth at $\omega = 0$, this is not a general symbol.

Since the symbol calculus for compositions of FIO assumes the operators are FIO and ΨDO with general symbols, we define a new operator $\mathcal{L}'$ that is a composition of such operators and calculate the symbol of the composition. Then, we show $\mathcal{L}' - \mathcal{L}$ is smoothing. Therefore, $\sigma(\mathcal{L}) = \sigma(\mathcal{L}')$ by Definition 2.10.

Let $g \in \psi F \mathcal{E}'(X)$. We now characterize $\Sigma(g)$. For $g \in \mathcal{E}'(Y)$, $\Sigma(g)$ is the projection of $\mathrm{WF}(g)$ onto the cotangent coordinates (see Definition 2.2 and [14, Proposition 8.1.3]). As noted after Definition 2.2, the Fourier transform $\mathcal{F}g$ is rapidly decaying at ∞ in all closed cones in the complement of $\Sigma(g)$.

From (17), we see that the map $\Pi_{\mathrm{L}}\colon C \to T^*(Y)$ is given by

$$S \times X \times (\mathbb{R}\backslash\{0\}) \ni (s, \boldsymbol{x}, \omega) \mapsto (s, \varphi(s, \boldsymbol{x}), -\omega \partial_s \varphi(s, \boldsymbol{x}), \omega) \in T^*(Y). \tag{23}$$

The set

$$T' = \mathrm{Cl}\left(-\partial_s \varphi(\mathrm{Cl}(S \times X))\right)$$

is a compact subset of $\mathbb{R}$ because $\mathrm{Cl}(S \times X)$ is compact. Let

$$V' = \{(\tau, \omega) \in \mathbb{R} \times (\mathbb{R}\backslash\{0\}) : \ \pm \tau/\omega \in T'\}.$$

Then,

$$\Pi_{\mathrm{L}} \Pi_{\mathrm{R}}^{-1}(T^*(X)\backslash\{\mathbf{0}\}) \subset S \times T \times V'$$

which yields

$$\forall f \in \mathcal{E}'(X): \ \Sigma(\psi F f) \subset V' \tag{24}$$

by the Hörmander-Sato Lemma, see (11), and [14, Proposition 8.1.3].

To define the ΨDO $\mathcal{L}'$, we first specify a ΨDO M with general symbol that differs from $\mathrm{Id} \otimes L$ by a smoothing operator at least for $g \in \psi F \mathcal{E}'(X)$.

Let $v\colon \mathbb{R}^2\backslash\{\mathbf{0}\} \to \mathbb{R}$ be a smooth function homogeneous of degree zero, equal to 1 on an open conic neighborhood, V'', of V', *and* equal to 0 in an open conic neighborhood of $\{\omega = 0\}$. This is possible because V' and $\{\omega = 0\}$ are disjoint closed conic subsets of $\mathbb{R}^2\backslash\{\mathbf{0}\}$. Then,

$$m(s, t, \tau, \omega) = v(\tau, \omega)\ell(\omega)$$

is a general symbol of order $\max(0, \mathrm{Order}(L))$ because it is smooth for $(\tau, \omega) \neq \mathbf{0}$ since it is 0 in a conic neighborhood of $\{\omega = 0\}$ in $\mathbb{R}^2\backslash\{\mathbf{0}\}$. Let M be the ΨDO with general symbol m.

Let $\psi' \in \mathcal{D}(S)$ and equal to one on an open neighborhood of $\mathrm{supp}(\psi)$. Then,

$$\mathcal{L}' = \frac{1}{2\pi} F_W^\dagger (\psi' M) \psi F\colon \mathcal{E}'(X) \to \mathcal{D}'(X).$$

This is true because, if $f \in \mathcal{E}'(X)$, $\psi' M \psi F f$ is 0 if $s \notin \mathrm{supp}(\psi')$ so $F_W^\dagger$ can be composed with $\psi' M \psi F$. The operator $\mathcal{L}'$ is a ΨDO with general symbol because it is the composition of FIO and the ΨDO $\psi' M \psi$ that has a general symbol. The composition has canonical relation[3]

$$C^\top \circ \Delta_{T^*(S\times\mathbb{R})} \circ C \subset \Delta_{T^*(X)}$$

by the Bolker condition.

We will now calculate the symbol of $\mathcal{L}'$. The symbol calculations in Section 5.2 of [8] apply to our operators since $F_W^\dagger$ and F are generalized Radon transforms integrating over curves $t = \varphi(s, \boldsymbol{x})$ that satisfy the same assumptions as in [8], including the Bolker condition, and M is a general ΨDO.

We first calculate the principal symbols of $F_W^\dagger$ and $M\psi F$ at each point in $\Pi_{\mathrm{R}}^{-1}\{(\boldsymbol{x}, \xi)\}$ or, equivalently each coordinate $(s, \omega, \boldsymbol{x})$ for $(s, \omega) \in \mathcal{I}(\boldsymbol{x}, \xi)$. The principal symbols of $F^*\psi'$ and ψF are calculated between equations (5.19) and (5.20) of [8] where we must replace A_3 in the principal symbol for F^* by $W\psi'$ to get the principal symbol of $F_W^\dagger \psi'$.

To calculate the principal symbol of $M\psi F$ at $(s, \boldsymbol{x}, \omega)$, we evaluate $m(s, t, \tau, \omega)\psi(s)$ at the image of this point in C to get $m(s, \varphi(s, \boldsymbol{x}), -\omega\partial_s\varphi, \omega)$ (because (23) gives the image in $T^*(Y)$ of $(s, \boldsymbol{x}, \omega)$ under Π_{L}), use that $t = \varphi(s, \boldsymbol{x})$), and then multiply by the principal symbol of ψF from [8]. Then, for each $(s, \omega) \in \mathcal{I}(\boldsymbol{x}, \xi)$, one multiplies the two principal symbols (with m in the middle). The calculation of the denominator of the product principal symbol in [8, Lemma 5.1] is for a Radon transform on two-dimensional surfaces, and it involves ω^2. The same calculation for a transform like ours, which integrates over curves (which are one-dimensional) gives a factor of $|\omega|$, as in [16, Section 3].

[3]Here, $\Delta_{T^*(Z)} \subset T^*(Z) \times T^*(Z)$ denotes the diagonal (identity relation).

By Lemma 3.1, $\mathcal{I}(\boldsymbol{x},\xi)$ is a finite set. To calculate the principal symbol of $\mathcal{L}'$ at $(\boldsymbol{x},\xi) \in T^*(X)\backslash\{\mathbf{0}\}$, one adds up the finite number of preimages under Π_{R} of $(\boldsymbol{x},\xi)$ (equivalently: points in $\mathcal{I}(\boldsymbol{x},\xi)$) (see, e.g., [16, equation (3.29)]), and the result is (20) where $\ell(\omega)$ is replaced by $m(s,\varphi(s,\boldsymbol{x}),-\omega\partial_s\varphi(s,\boldsymbol{x}),\omega)$.

We now show $\mathcal{L}'-\mathcal{L}$ is smoothing on $\mathcal{E}'(X)$. We first validate that the operator $M-\mathrm{Id}\otimes L$ is smoothing for all distributions in $\psi F\mathcal{E}'(X)$. Note that this is not completely trivial because $\sigma(M-\mathrm{Id}\otimes L)=(v(\tau,\omega)-1)\ell(\omega)$ is a singular symbol on $\mathcal{E}'(Y)$ since it is not smooth for $\omega=0$, so this operator is not a ΨDO.

Let $f\in\mathcal{E}'(X)$ and $g=\psi Ff$. Then, $\Sigma(g)\subset V'$ by (24). Furthermore,

$$(M-\mathrm{Id}\otimes L)g=\mathcal{F}^{-1}\left((v(\tau,\omega)-1)\ell(\omega)\mathcal{F}g\right) \tag{25}$$

is a multiplier on the Fourier transform that is zero on a neighborhood of V'. By (24), the product inside (25) is rapidly decaying in all directions, and $(M-\mathrm{Id}\otimes L)g$ is smooth. Since Mg is defined, this shows that $(\mathrm{Id}\otimes L)g$ is defined.

Since $(M-\mathrm{Id}\otimes L)\psi Ff$ is smooth for $f\in\mathcal{E}'(X)$, the operator

$$(\mathcal{L}'-\mathcal{L})=\frac{1}{2\pi}F_W^{\dagger}\psi'(M-\mathrm{Id}\otimes L)\psi F\colon\ \mathcal{E}'(X)\to\mathcal{D}'(X) \tag{26}$$

is smoothing. Note that we use (21) and that $\psi'\psi=\psi$ in (26). By Definition 2.10, $\sigma(\mathcal{L})=\sigma(\mathcal{L}')$ and (20) is justified. □

We point out that our symbol calculations and those in [8, 16] follow from calculations in [19] and fundamental results [13, (2.4.2) and Theorems 2.4.2 and 4.2.3], all of which use the definition of principal symbol at the end of Definition 2.10.

3.2. **Filtered normal operators.** The imaging operators we consider in this subsection are products of a generalized normal operator with a pseudodifferential operator which basically performs a 2D frequency filtering:

$$\Lambda=\frac{1}{2\pi}KF_W^{\dagger}\psi F$$

where K is a properly supported general pseudodifferential operator of order $\kappa\geq 1$ and $\psi\in\mathcal{D}(S)$ is a cutoff function. Note that Λ is of the non-negative order $\kappa-1$.

Remark 3.3. *The definition of Λ is inspired by the inversion formula,*

$$u=\frac{1}{2\pi}(-\Delta)^{1/2}R^*Ru,\quad u\in\mathcal{E}'(\mathbb{R}^2),$$

for the classical Radon transform from Example 2.11. Here, $(-\Delta)^{1/2}$ is the general pseudodifferential operator with full symbol $|\xi|$. Thus, the above inversion formula follows directly from (13) or see, e.g., [12, Chapter I, Theorem 3.1].

Assume the zero-offset scanning geometry where source and receiver positions coincide:

$$\boldsymbol{x_s}(s)=\boldsymbol{x_r}(s)=(s,0)^{\top},\quad s\in\mathbb{R}. \tag{27}$$

Then, F given by (16) satisfies the Bolker condition (see Definition 2.8) for a constant and an affine-linearly increasing background velocity v where $\mathcal{X}=\mathbb{R}^2_+$, see [4] and [16], respectively. According to Theorem 3.2, $\Lambda\colon\ \mathcal{E}'(X)\to\mathcal{D}'(X)$ is a general pseudodifferential operator for any $X\Subset\mathbb{R}^2_+$ with principal symbol

$$\sigma(\Lambda)(\boldsymbol{x},\xi)=k(\boldsymbol{x},\xi)\sum_{(s,\omega)\in\mathcal{I}(\boldsymbol{x},\xi)}\frac{\psi(s)W(s,\boldsymbol{x})A(s,\boldsymbol{x})}{|\omega B(s,\boldsymbol{x})|}.$$

Setting, for instance,

$$W(s,\boldsymbol{x}) = \frac{|B(s,\boldsymbol{x})|}{A(s,\boldsymbol{x})\,|\nabla_{\boldsymbol{x}}\varphi(s,\boldsymbol{x})|} \tag{28}$$

we get

$$\sigma(\Lambda)(\boldsymbol{x},\xi) = \frac{k(\boldsymbol{x},\xi)}{|\xi|} \sum_{(s,\omega)\in\mathcal{J}(\boldsymbol{x},\xi)} \psi(s). \tag{29}$$

In the sequel we consider two variants of Λ with weight (28):

$$\Lambda^{(i)} := \frac{1}{2\pi}\,(-\Delta)^{i/2} F^{\dagger}_{|B|/(A|\nabla_{\boldsymbol{x}}\varphi|)}\psi F, \quad i\in\{1,2\},$$

where $(-\Delta)^{i/2}$ is the general pseudodifferential ($i=1$) or differential ($i=2$) operator with full symbol $|\xi|^i$.

We now analyze the symbols of our basic operators.

Lemma 3.4. *Under the zero-offset scanning geometry (27), the principal symbol of $\Lambda^{(i)}$, $i\in\{1,2\}$, is*

$$\sigma(\Lambda^{(i)})(\boldsymbol{x},\xi) = |\xi|^{i-1} \sum_{(s,\omega)\in\mathcal{J}(\boldsymbol{x},\xi)} \psi(s).$$

So, $\Lambda^{(i)}$ has order $i-1$.

If $v(\cdot)=b>0$, then, for $\xi_2\neq 0$,

$$\sigma(\Lambda^{(i)})(\boldsymbol{x},\xi) = |\xi|^{i-1}\,\psi\Big(x_1 - \frac{\xi_1}{\xi_2}\,x_2\Big). \tag{30}$$

If $v(\boldsymbol{x}) = ax_2+b$, $a,b>0$, then

$$\sigma(\Lambda^{(i)})(\boldsymbol{x},\xi) = |\xi|^{i-1}\begin{cases} \psi(s_-)+\psi(s_+) & :\ \xi_1\neq 0,\\ \psi(x_1) & :\ \xi_1 = 0,\end{cases} \tag{31}$$

where

$$s_\pm = s_\pm(\boldsymbol{x},\xi) = x_1 + \frac{\xi_2}{\xi_1}\,\frac{b+ax_2}{a} \pm \sqrt{\frac{x_2}{a}(2b+ax_2) + \Big(\frac{\xi_2}{\xi_1}\,\frac{b+ax_2}{a}\Big)^2}.$$

Proof. The general expression for the symbol follows readily from (28) and (29) with $k(\boldsymbol{x},\xi) = |\xi|^i$. To get the representations of $\sigma(\Lambda^{(i)})$ for both concrete wave speeds we use the explicit characterizations of the respective sets $\mathcal{J}(\boldsymbol{x},\xi)$ given in [8, Lemma 3.6] and [16, equation (3.28)]. □

Remark 3.5. *Taking the pointwise limit of the symbol (31) for $\xi_2\neq 0$ as $a\searrow 0$ yields the symbol (30).*

We now consider constant velocity. Because the symbol (30) is not elliptic, we cannot expect to recover all singularities of u from $\Lambda^{(i)}u$. Our next corollary shows how to do this if we limit $\mathrm{WF}(u)$.

Corollary 3.6. *Let $v(\cdot)=b>0$ and assume the zero-offset scanning geometry (27). To any open $X\Subset\mathcal{X}$ and any cone $V=\{\eta\in\mathbb{R}^2\backslash\{0\} : |\eta_1|\le M|\eta_2|\}$, $M>0$, there are an open $S\Subset\mathcal{S}$, a cutoff function $\psi\in\mathcal{D}(S)$, and general pseudodifferential operators $O^{(i)}$, $i\in\{1,2\}$, such that*

$$\Lambda^{(1)}u = u + O^{(1)}u \quad \textit{and} \quad \Lambda^{(2)}u = (-\Delta)^{1/2}u + O^{(2)}u, \tag{32}$$

for all $u \in \mathcal{E}'(X)$ with $\mathrm{WF}(u) \subset X \times V$. For those u, $O^{(1)}u$ is one degree smoother in Sobolev scale than u and $O^{(2)}u$ is one degree smoother in Sobolev scale than $(-\Delta)^{1/2}u$.

Proof. Let $P^{(i)}$ be the general pseudodifferential operator with full symbol $\sigma(\Lambda^{(i)})$. Then, by the definition of a principal symbol, we may write $\Lambda^{(i)} = P^{(i)} + Q^{(i)}$ where $Q^{(i)}$ has order $i-2$ since $P^{(i)}$, the principal symbol of $\Lambda^{(i)}$, has order $i-1$ (see Definition 2.10).

The set

$$D = \big\{x_1 - q\, x_2 : \boldsymbol{x} \in \mathrm{Cl}(X),\ \xi \in V,\ q = \xi_1/\xi_2\big\}$$

is compact in $\mathbb{R}$. Then, there are an open $S \Subset \mathbb{R}$, that contains D, a $\psi \in \mathcal{D}(S)$ with $\psi \geq 0$ and $\psi = 1$ in a neighborhood of D, so that $\sigma(\Lambda^{(i)})|_{X\times V} = |\xi|^{i-1}$.

Let $u \in \mathcal{E}'(X)$ with $\mathrm{WF}(u) \subset X \times V$. We split

$$P^{(i)}u = (-\Delta)^{(i-1)/2}u + R^{(i)}u \quad \text{where } R^{(i)} := P^{(i)} - (-\Delta)^{(i-1)/2}$$

and have that

$$R^{(i)}u(\boldsymbol{y}) = \frac{1}{4\pi^2}\int_{\mathbb{R}^2\setminus V}\int_X \big(\sigma(\Lambda^{(i)})(\boldsymbol{x},\xi) - |\xi|^{i-1}\big)\, u(\boldsymbol{x})\, \mathrm{e}^{\imath\,(\boldsymbol{y}-\boldsymbol{x})^\top\xi}\mathrm{d}\boldsymbol{x}\,\mathrm{d}\xi. \tag{33}$$

Moreover, the decompositions in (32) hold for $O^{(i)} := Q^{(i)} + R^{(i)}$, $i = 1, 2$.

Using (33), (30), and the choice of ψ, one sees that the full symbol of $R^{(i)}$ is zero in a neighborhood of $X \times V$. This says that $\mathrm{WF}(R^{(i)}u) \subset X \times (\mathbb{R}^2\setminus V)$. However, by assumption, $\mathrm{WF}(R^{(i)}u) \subset \mathrm{WF}(u) \subset X \times V$. Therefore, $R^{(i)}u$ is a smooth function. Since $Q^{(i)}$ has order $i-2$, and $\Lambda^{(i)}$ has order $i-1$, we conclude that $O^{(1)}u$ is one degree smoother in Sobolev scale than u and $O^{(2)}u$ is one degree smoother in Sobolev scale than $(-\Delta)^{1/2}u$. □

3.3. **Traditional Kirchhoff operators.** The 2D Kirchhoff migration schemes described in formulas (5.1.40) and (5.1.41) of [2] can be expressed by the following imaging operators

$$\mathrm{I}_{\mathrm{K}}^{(1)} = \frac{1}{2\pi}\, F^\dagger_{|B|/A}\big(\mathrm{Id}\otimes(H\partial)\big)\psi F \quad \text{and} \quad \mathrm{I}_{\mathrm{K}}^{(2)} = \frac{1}{2\pi}\, F^\dagger_{|B|/(v^2A|\nabla_{\boldsymbol{x}}\varphi|)}\big(\mathrm{Id}\otimes(H\partial^2)\big)\psi F,$$

respectively. Here, H denotes the Hilbert transform and ∂ is the first order differential operator. These operators commute: $H\partial = \partial H$. The cutoff function ψ is as in the previous subsection and introduced for the same reason. It does not appear in the original formulas of [2].

Remark 3.7. *The operator $\mathrm{I}_{\mathrm{K}}^{(1)}$ resembles the filtered backprojection inversion formula*

$$u = \frac{1}{2\pi}\, R^*\big(\mathrm{Id}\otimes(H\partial)\big)Ru, \quad u \in \mathcal{E}'(\mathbb{R}^2),$$ [4]

of the classical Radon transform from Example 2.11, see, e.g., [12, Chapter I, Theorem 3.8].

Under the Bolker condition, the operators $\mathrm{I}_{\mathrm{K}}^{(1)}$ and $\mathrm{I}_{\mathrm{K}}^{(2)}$ are general pseudodifferential operators with orders 0 and 1, respectively. In view of Theorem 3.2 and using $\sigma(H\partial)(t,\omega) = |\omega|$ as well as $\sigma(H\partial^2)(t,\omega) = -\imath|\omega|\omega$, the principal symbols read

$$\sigma(\mathrm{I}_{\mathrm{K}}^{(1)})(\boldsymbol{x},\xi) = \sum_{(s,\omega)\in\mathcal{J}(\boldsymbol{x},\xi)} \psi(s) \tag{34}$$

[4] The operator $H\partial$ acts on the lateral variable of Ru.

and

$$\sigma(\mathrm{I}_{\mathrm{K}}^{(2)})(\boldsymbol{x},\xi) = -\imath\,\frac{1}{|\xi|}\,\frac{1}{v(\boldsymbol{x})^2}\sum_{(s,\omega)\in\mathcal{J}(\boldsymbol{x},\xi)}|\omega|\,\omega\,\psi(s) \tag{35}$$

$$= -\imath\,\frac{|\xi|}{v(\boldsymbol{x})^2}\sum_{(s,\omega)\in\mathcal{J}(\boldsymbol{x},\xi)}\operatorname{sgn}(\omega)\,\frac{\psi(s)}{|\nabla_{\boldsymbol{x}}\varphi(s,\boldsymbol{x})|^2}.$$

An analogue of Corollary 3.6 holds for $\mathrm{I}_{\mathrm{K}}^{(1)}$.

Corollary 3.8. *Let $v(\cdot) = b > 0$ and assume the zero-offset scanning geometry (27). To any open $X \Subset \mathcal{X}$ and any cone $V = \{\eta \in \mathbb{R}^2\backslash\{0\} : |\eta_1| \le M|\eta_2|\}$, $M > 0$, there are an open $S \Subset \mathcal{S}$, a cutoff function $\psi \in \mathcal{D}(S)$, and a general pseudodifferential operator O_{K} such that*

$$\mathrm{I}_{\mathrm{K}}^{(1)}\,u = u + O_{\mathrm{K}}u$$

for all $u \in \mathcal{E}'(X)$ with $\mathrm{WF}(u) \subset X \times V$. For those u, $O_{\mathrm{K}}u$ is one degree smoother in Sobolev scale than u.

Proof. Since

$$\sigma(\mathrm{I}_{\mathrm{K}}^{(1)})(\boldsymbol{x},\xi) = \sigma(\Lambda^{(1)})(\boldsymbol{x},\xi)$$

we can follow the argumentation of the proof of Corollary 3.6. □

In fact, both operators $\Lambda^{(1)}$ and $\mathrm{I}_{\mathrm{K}}^{(1)}$ deliver similar reconstructions for a constant background velocity model, see Figure 1.

Remark 3.9. *In [2] the migration formula based on $\mathrm{I}_{\mathrm{K}}^{(2)}$ was introduced to "image discontinuities" of n, that is, to recover the reflectivity function which "consists of bandlimited delta functions having peak amplitudes occurring at reflector locations" (quotes from [2, p. 88]). Our analysis of its principal symbol shows that the operator indeed provides what is wanted since it is of order 1. However, the factor $1/v(\boldsymbol{x})^2$ in $\sigma(\mathrm{I}_{\mathrm{K}}^{(2)})$ de-emphasizes features at locations with a high background velocity. Of course, this disadvantage can easily be corrected by choosing the weight (28) in the backprojection of $\mathrm{I}_{\mathrm{K}}^{(2)}$.*

Remark 3.10. *For $v(\cdot) = 1$, Beylkin [1, (4.13)] proposed the imaging operator*

$$\mathrm{I}_{\mathrm{B}} = \frac{1}{\pi}F^{\dagger}_{|B|/A}(\mathrm{Id}\otimes K)\psi F \tag{36}$$

where K is a convolution in time with kernel $\kappa(t) = (2\pi)^{-d/2}\int_0^\infty \omega^{d-1}\mathrm{e}^{\imath t\omega}\mathrm{d}\omega$ (d is the dimension of the ambient space). We have again added the cutoff function ψ. Beylkin showed the splitting

$$\mathrm{I}_{\mathrm{B}} = \mathrm{Id}_{\mathrm{part}} + \mathrm{S}$$

with the partial identity $\mathrm{Id}_{\mathrm{part}}$, which is essentially a lowpass filter, and a smoothing operator S.

To interpret I_{B} for $d = 2$ in our framework as a general pseudodifferential operator we insert the Heaviside function χ into the Fourier integral defining κ. This function satisfies $\chi(\omega) = 0$ for $\omega < 0$ and $\chi(\omega) = 1$ for $\omega \ge 0$. We denote the resulting operator by $\mathrm{I}_{\mathrm{B},\chi}$. Then, by applying

Theorem 3.2,

$$\sigma(\mathrm{I}_{\mathrm{B},\chi})(\boldsymbol{x},\xi) = \frac{2}{|\xi|}\sum_{(s,\omega)\in\mathcal{I}(\boldsymbol{x},\xi)}\chi(\omega)|\omega|\psi(s)$$
$$= 2\sum_{(s,\omega)\in\mathcal{I}(\boldsymbol{x},\xi)}\chi\Big(\frac{|\xi|^2}{\xi^\top\nabla_{\boldsymbol{x}}\varphi(s,\boldsymbol{x})}\Big)\frac{\psi(s)}{|\nabla_{\boldsymbol{x}}\varphi(s,\boldsymbol{x})|}.$$

Hence, the action of $\mathrm{I}_{\mathrm{B},\chi}$*, that is, of* I_{B}*, and the actions of* $\mathrm{I}_{\mathrm{K}}^{(1)}$ *and* $\Lambda^{(1)}$ *on real-valued distributions are virtually identical in case of* $v(\cdot)=1$ *under the zero-offset scanning geometry: Let* $\xi\in\mathbb{R}^2$ *with* $\xi_2\neq 0$*. In view of* (30) *we obtain*

$$\sigma(\mathrm{I}_{\mathrm{B},\chi})(\boldsymbol{x},\xi) = \chi\Big(\frac{|\xi|^2}{\xi^\top\nabla_{\boldsymbol{x}}\varphi(x_1-q\,x_2,\boldsymbol{x})}\Big)\,\psi(x_1-qx_2)$$

where $q=\xi_1/\xi_2$*. Now, assume* $\xi^\top\nabla_{\boldsymbol{x}}\varphi(x_1-q\,x_2,\boldsymbol{x})<0$ *so that* $\sigma(\mathrm{I}_{\mathrm{B},\chi})(\boldsymbol{x},\xi)=0$*. For a real-valued distribution* u*, if* $(\boldsymbol{x},\xi)\in\mathrm{WF}(u)$ *then* $(\boldsymbol{x},-\xi)\in\mathrm{WF}(u)$ *and*

$$\sigma(\mathrm{I}_{\mathrm{B},\chi})(\boldsymbol{x},-\xi) = \sigma(\Lambda^{(1)})(\boldsymbol{x},\pm\xi)$$

We conclude that $\mathrm{I}_{\mathrm{B},\chi}\,u$ *and* $\Lambda^{(1)}u$ *display the same part of the singular support of* u*.*

4. Numerical scheme

Our numerical schemes for the $\Lambda^{(i)}$'s and the $\mathrm{I}_{\mathrm{K}}^{(i)}$'s, $i\in\{1,2\}$, are based on the concept of approximate inverse [17, 23]. To this end let, for $k>0$,

$$e_\gamma(\boldsymbol{x}) = \frac{k+1}{\pi\,\gamma^{2(k+1)}}\begin{cases}(\gamma^2-|\boldsymbol{x}|^2)^k: & |\boldsymbol{x}|<\gamma,\\ 0 & : |\boldsymbol{x}|\geq\gamma.\end{cases} \tag{37}$$

The family $\{e_\gamma\}_{\gamma>0}$ converges to δ in the distributional sense as $\gamma\to 0$. In our computations in the next section, we always set $k=3$.

Now, for $\boldsymbol{p}\in X$ and $g\in L^2(Y)$, we define the approximate inverse for $\Lambda^{(i)}$ by

$$L_\gamma^{(i)}g(\boldsymbol{p}) := \langle\psi g, v_{\boldsymbol{p},\gamma}^{(i)}\rangle_{L^2(Y)}$$

where, for W as in (28),

$$v_{\boldsymbol{p},\gamma}^{(i)}(s,t) = \frac{1}{2\pi}\widetilde{F}\big(W(s,\cdot)(-\Delta)^{i/2}e_\gamma(\cdot-\boldsymbol{p})\big)(s,t) \tag{38}$$

is the *reconstruction kernel* and

$$\widetilde{F}\rho(s,t) = \int_{\mathcal{L}_{(s,t)}}\rho(s,\boldsymbol{x})\,\frac{\mathrm{ds}(\boldsymbol{x})}{|\nabla_{\boldsymbol{x}}\varphi(s,\boldsymbol{x})|}, \tag{39}$$

where $\mathcal{L}_{(s,t)}$ is the isochrone defined in (7), see [6] for implementation details. Note that the following convolution product holds

$$L_\gamma^{(i)}Fn(\boldsymbol{p}) = \Lambda^{(i)}n\star e_\gamma(\boldsymbol{p})$$

which explains the name "approximate inverse": we recover a smoothed version of $\Lambda^{(i)}n$ from the data $g=Fn$.

Remark 4.1. *In the definition* (38) *of the kernel, the expression* $(-\Delta)^{i/2}e_\gamma$ *appears. For* $i=2$ *this expression can easily by computed analytically and even for* $i=1$ *we have a closed form in terms of the hypergeometric function, see Appendix* A.

The approximate inverse $J_\gamma^{(i)}$ of $\mathrm{I}_\mathrm{K}^{(i)}$ is obtained in the same way and likewise satisfies

$$J_\gamma^{(i)} Fn(\boldsymbol{p}) = \mathrm{I}_\mathrm{K}^{(i)} n \star e_\gamma(\boldsymbol{p}).$$

One only has to adapt the definition of the reconstruction kernel, for instance, we get

$$v_{\boldsymbol{p},\gamma}^{(1)}(s,t) = \frac{1}{2\pi}(\mathrm{Id}\otimes H\partial)\widetilde{F}\big(|B(s,\cdot)|e_\gamma(\cdot-\boldsymbol{p})/A(s,\cdot)\big)(s,t).$$

5. Computational experiments

We compare numerical realizations of $L_\gamma^{(i)} Fn$ and $J_\gamma^{(i)} Fn$, $i = 1, 2$, for

$$n = \chi_{B_2((0,5),2)} - \chi_{B_2((0,5),1)} + \chi_{B_\infty((3,6),1.25)} + \chi_{\{\boldsymbol{x}\in\mathbb{R}^2_+ :\, x_2 \geq 6.5+\sin(\pi x_1/2)\}}, \tag{40}$$

which is composed of indicator functions of circular and rectangular disks and of a half space with a sine-like boundary, see top of Figure 1.

Our code in the Python programming language, with which we have performed all numerical experiments, is published in [5].

5.1. Consistent data.

The data Fn we use here are computed numerically by the algorithm explained in [6].

In our first experiment we illustrate the statements of Corollaries 3.6 and 3.8. To this end we use the constant background velocity model $v(\cdot) = 1$ and the zero-offset scanning geometry (27). Here, $t_{\text{first}}(s) = 0$ for any s and the Bolker condition is satisfied in $\mathcal{X} = \mathbb{R}^2_+$, see [4]. Note that wave fronts $(\boldsymbol{y}, \xi)$ of n with $\xi_2 = 0$ are neither visible in $\Lambda^{(1)} n$ nor in $\mathrm{I}_\mathrm{K}^{(1)} n$ (whatever ψ and S are chosen), see [9, Theorem 3.9]. For the computations of $L_{0.2}^{(1)} Fn$ and $J_{0.2}^{(1)} Fn$, shown on the bottom of Figure 1, ψ and $Y \subset S \times (0, t_{\max})$ have been designed so that the assertions of both corollaries hold for Ω being the image section displayed and for a cone C which also contains directions being very close to the horizontal line. Hence, we expect and indeed observe that $L_{0.2}^{(1)} Fn \approx n \approx J_{0.2}^{(1)} Fn$ except at locations where n has a singularity that is close to the horizontal direction. For a quantitative comparison of both reconstructions we give pixel-based relative errors in Table 1.

	$L_{0.2}^{(1)} Fn$	$J_{0.2}^{(1)} Fn$
ℓ^2-norm	42%	61%
ℓ^∞-norm	79%	95%

TABLE 1. Relative errors with respect to n of the reconstructions shown in Figure 1.

For the next set of experiments, the GRT F is given with respect to the linear background velocity model

$$v(\boldsymbol{x}) = 0.1 x_2 + 0.5 \tag{41}$$

and the common offset scanning geometry:

$$\boldsymbol{x_s}(s) = (s-\alpha, 0)^\top \quad \text{and} \quad \boldsymbol{x_r}(s) = (s+\alpha, 0)^\top$$

where $\alpha > 0$ is the offset. We use $\alpha = 5$, if not stated otherwise. In this scenario the Bolker condition (see Definition 2.8) holds for

$$\mathcal{X} = \{\boldsymbol{x} \in \mathbb{R}^2_+ : x_2 > x_{\min}\} \text{ where } x_{\min} \approx 2.07 \text{ and } t_{\text{first}}(s) \approx 17.63$$

for all s, see [16, Section 3]. Note that $\operatorname{supp} n \subset \mathcal{X}$. Moreover, the whole singular support of n can be reconstructed by all of our imaging operators, provided ψ and Y, that is, S, are chosen appropriately, see [16, Proposition 3.5 and Remark 3.7].

On the top right of Figure 2 a numerical approximation to $L_{0.2}^{(2)} Fn$ is displayed. Note that $\Lambda^{(2)}$ is a pseudodifferential operator of order 1 and so the singular support of n is emphasized

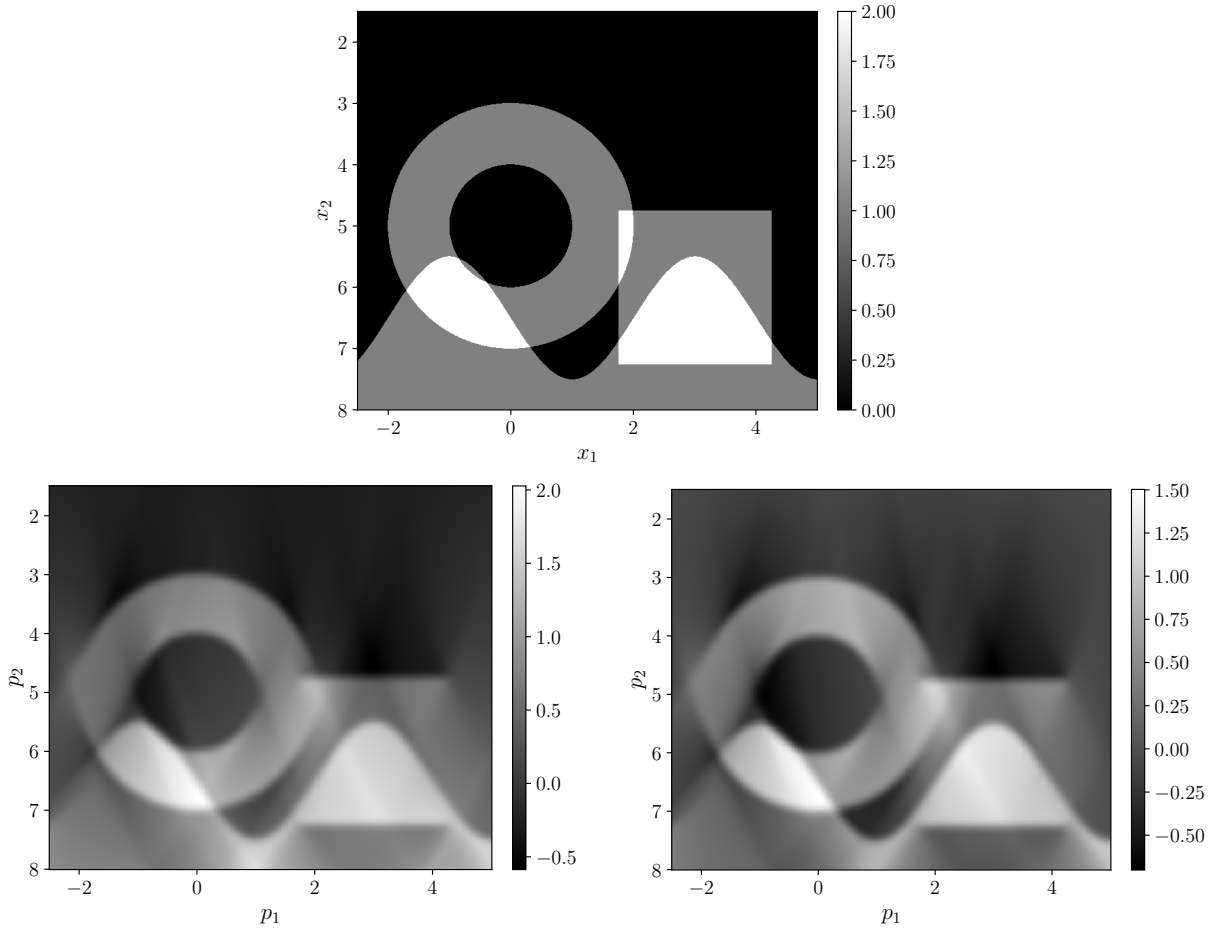

FIGURE 1. Top: Illustration of the function n from (40) with the following color code: black, grey, and white indicate the numerical values 0, 1, and 2, respectively.
Bottom: $L^{(1)}_{0.2}Fn$ (left), $J^{(1)}_{0.2}Fn$ (right) for the zero-offset scanning geometry (27) and background velocity $v(\cdot) = 1$. Note the different gray scales. Relative error values are listed in Table 1.

in $L^{(2)}_{0.2}Fn$. In contrast, the operator $\Lambda^{(1)}$ has order 0, see Figure 2 (top left) for the resulting image which is a quite good reconstruction of n, both in qualitative and quantitative terms.

The middle row of Figure 2 shows numerical approximations to $J^{(1)}_{0.2}Fn$ (left) and $J^{(2)}_{0.2}Fn$ (right) where the corresponding Kirchhoff operators are $\mathrm{I}^{(1)}_{\mathrm{K}}$ and $\mathrm{I}^{(2)}_{\mathrm{K}}$, respectively. The reconstruction $J^{(1)}_{0.2}Fn$ is close to $L^{(1)}_{0.2}Fn$ (top left). The singular support of n is visible in $J^{(2)}_{0.2}Fn$ but the strength of the displayed contrast/intensity at a reconstruction point depends on v, that is, on depth.

In view of the symbols (34) and (35) we notice that deleting the Hilbert transform from the definition of the $\mathrm{I}^{(i)}_{\mathrm{K}}$'s does not affect their orders, that is,

$$\widetilde{\mathrm{I}}^{(1)}_{\mathrm{K}} = \frac{1}{2\pi} F^{\dagger}_{|B|/A} \psi\big(\mathrm{Id} \otimes \partial\big) F \quad \text{and} \quad \widetilde{\mathrm{I}}^{(2)}_{\mathrm{K}} = \frac{1}{2\pi} F^{\dagger}_{|B|/(v^2 A|\nabla_{\boldsymbol{x}}\varphi|)} \psi\big(\mathrm{Id} \otimes \partial^2\big) F,$$

share the order with $\mathrm{I}^{(1)}_{\mathrm{K}}$ and $\mathrm{I}^{(2)}_{\mathrm{K}}$, respectively. Hence, we expect $\widetilde{\mathrm{I}}^{(i)}_{\mathrm{K}} n$ not to differ qualitatively much from $\mathrm{I}^{(i)}_{\mathrm{K}} n$. Our expectation is confirmed by the numerical approximations to

$$\widetilde{J}^{(i)}_{0.2} Fn = \widetilde{\mathrm{I}}^{(i)}_{\mathrm{K}} n \star e_{0.2}, \quad i \in \{1, 2\},$$

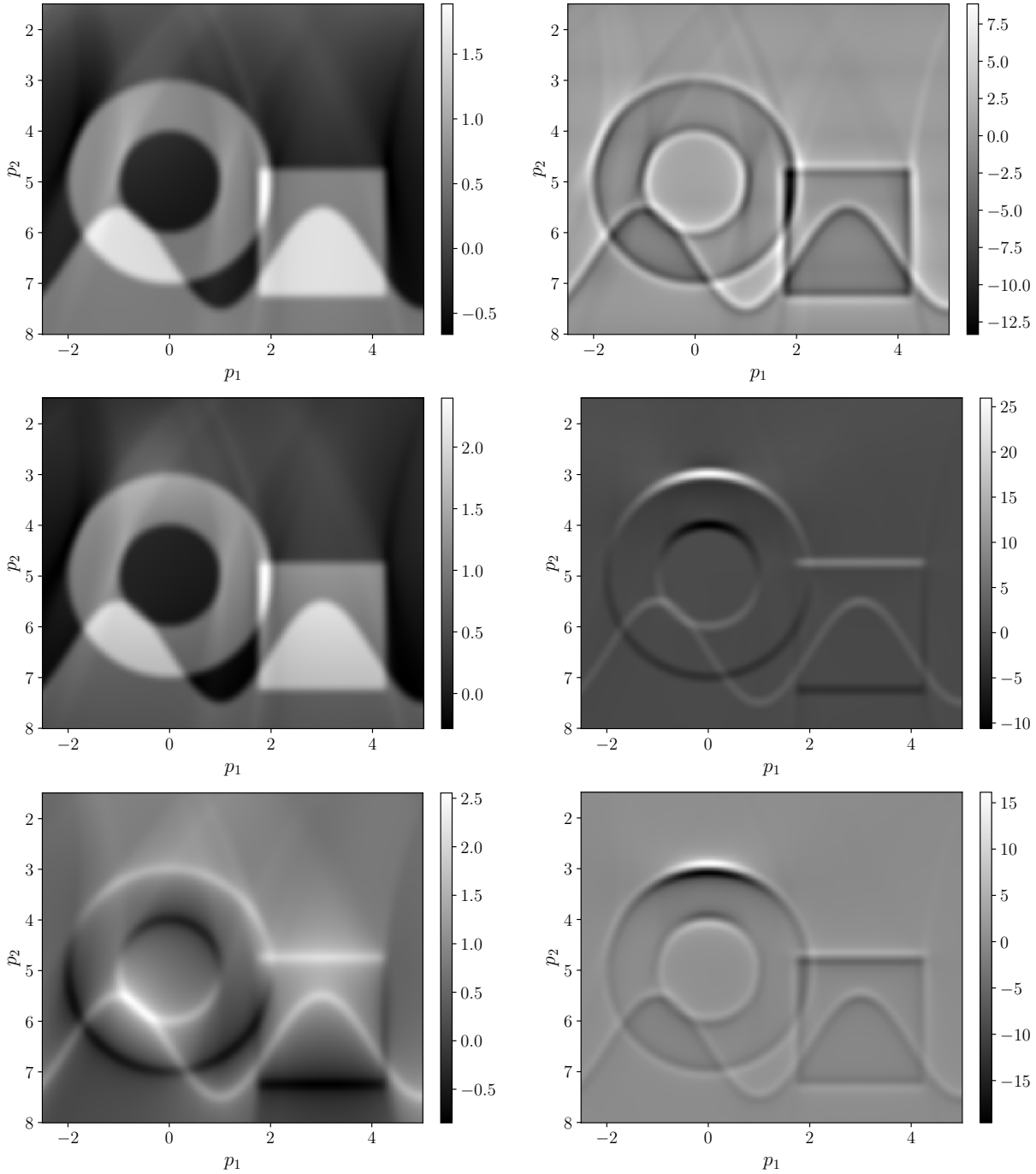

FIGURE 2. Reconstructions for the linear velocity model (41) and the common offset scanning geometry with $\alpha = 5$.
Top: $L^{(1)}_{0.2}Fn$ (left), $L^{(2)}_{0.2}Fn$ (right). Middle: $J^{(1)}_{0.2}Fn$ (left), $J^{(2)}_{0.2}Fn$ (right). Bottom: $\widetilde{J}^{(1)}_{0.2}Fn$ (left), $\widetilde{J}^{(2)}_{0.2}Fn$ (right).
As predicted by the theory in [16], the singular support of n within the displayed image section is visible for all imaging operators.

see bottom of Figure 2. In fact, both $J^{(i)}_{0.2}Fn$ and $\widetilde{J}^{(i)}_{0.2}Fn$ provide more or less the same microlocal information about n. As a conclusion, we can dispense with the (nonlocal) Hilbert transform in the Kirchhoff operator $\mathrm{I}^{(2)}_{\mathrm{K}}$.

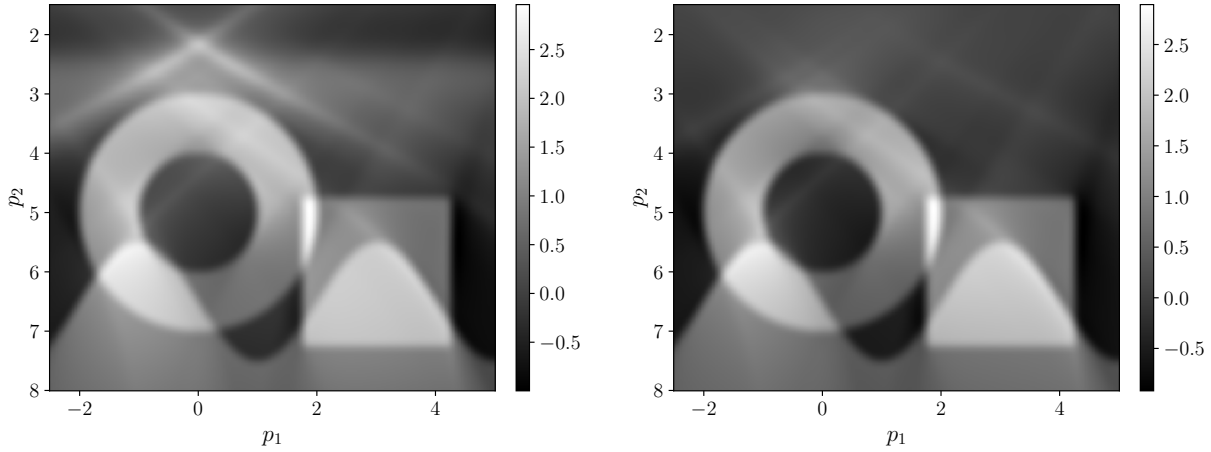

FIGURE 3. Reconstructions for the velocity model (42) which violates the geometric optics assumption. The underlying scanning geometry is common offset with $\alpha = 3$. Left: $L^{(1)}_{0.2}Fn$, right: $J^{(1)}_{0.2}Fn$.

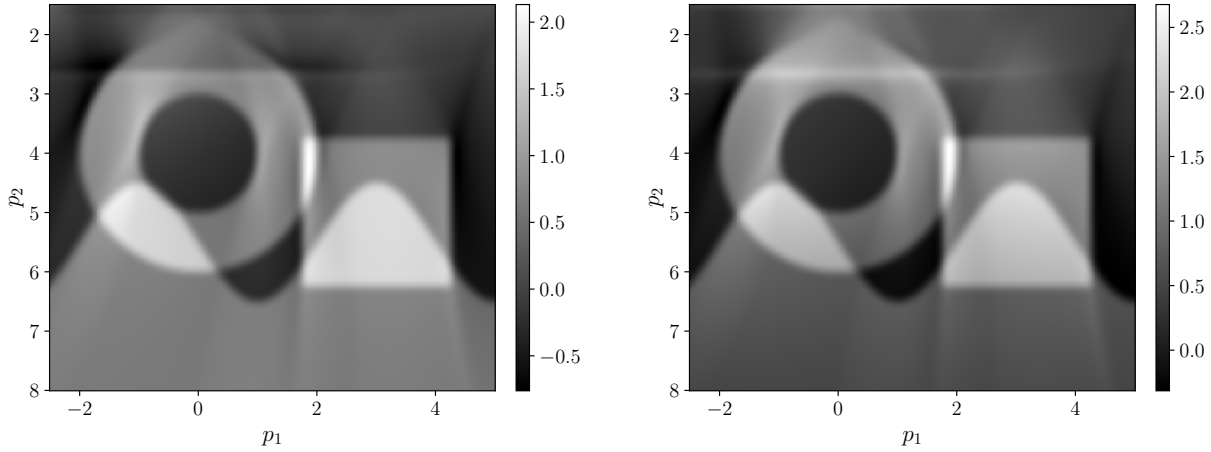

FIGURE 4. Reconstructions for the linear velocity model (41) and common offset scanning geometry with $\alpha = 5$ (these parameters are as in Figure 2). Left: $L^{(1)}_{0.2}Fn^*$, right: $J^{(1)}_{0.2}Fn^*$, where $n^*(x_1, x_2) = n(x_1, x_2 + 1)$ with n from (40).

We further observe that both, $\mathrm{I}^{(2)}_{\mathrm{K}}$ and $\widetilde{\mathrm{I}}^{(2)}_{\mathrm{K}}$, map jumps in n with same height but at different depths with different intensities. The larger x_2 is, the stronger this damping effect is pronounced, see Remark 3.9.

Both background velocities, which we used so far, satisfy the geometric optics assumption in contrast to

$$v(\boldsymbol{x}) = \frac{1}{2}\left(1 + x_2 + \frac{1}{2}\cos\left(\frac{\pi}{4}x_2\right)\right), \tag{42}$$

see [6]. Nevertheless, both reconstructions $L^{(1)}_{0.2}Fn$ and $J^{(1)}_{0.2}Fn$, displayed in Figure 3, yield good approximations to n for this strictly increasing background velocity where the artifacts in $L^{(1)}_{0.2}Fn$ are a bit stronger.

Finally, we consider a situation where the imaging operators $\Lambda^{(1)}$ and $\mathrm{I}^{(1)}_{\mathrm{K}}$ fail to be pseudodifferential operators. The object to be imaged is $n^*(x_1, x_2) = n(x_1, x_2 + 1)$ which is an upwards shifted version of n displayed at the top of Figure 1. It overlaps slightly with the strip

where the Bolker condition is violated ($0 < x_2 \leq x_{\min} \approx 2.07$). As a result, the reconstructions in Figure 4 suffer from a horizontal streak artifact at about $p_2 = 2.7$, which is slightly more pronounced for $\mathrm{I}_{\mathrm{K}}^{(1)}$. Note that the singularity $1/|\nabla\varphi(s,\boldsymbol{x})|$ at $\boldsymbol{x} = (x_1, x_{\min})^\top$ in F, compare the integrand of $\widetilde{F}$ in (39), is mitigated by the choice of the cutoff function ψ which we have designed to vanish for travel times $t \leq t_{\text{first}} + 0.1$. We refer to [6, Sec. 5] for the exact definition of ψ.

5.2. **Realistic measurement scenario.** In this subsection, we simulate a realistic measurement scenario. To this end, we generate the data (seismograms) by numerically solving the wave equation, record the data using the common source scanning geometry, randomly perturb the seismograms with noise, and use different source and detector positions for data generation and inversion.

The data g as input to $L_\gamma^{(i)}$ and $J_\gamma^{(i)}$ are generated by the right-hand side of (3), that is, we numerically solve the wave equation (1) for u and $\widetilde{u}$. In view of (2), we set

$$\nu_{\text{pr}}^2(\boldsymbol{x}) = \frac{v^2(\boldsymbol{x})}{1 + 0.05\, n(\boldsymbol{x})}$$

with the background velocity v from (41). Further, n is as in (40) and the factor 0.05 in front of n scales down the committed linearization error.

In (1) we replace the source term by a scaled and time-shifted Gaussian pulse. The resulting equation is then solved on the computational domain $[-10, 20] \times [0, 10]$ using the wave solver of the open source toolbox PySIT [3]. To suppress unphysical reflections, we have provided the computational domain with absorbing boundaries by a perfectly matched layer (PML), see [6, Sec. 5.2] for more details. With ν_{pr} and v as input for the wave solver, we compute seismograms for 3 sources and 41 receivers for each source. The exact source positions are

$$\boldsymbol{x}_{\boldsymbol{s}1} = (-5, 0)^\top, \quad \boldsymbol{x}_{\boldsymbol{s}2} = (0, 0)^\top, \quad \boldsymbol{x}_{\boldsymbol{s}3} = (8, 0)^\top. \tag{43}$$

The exact receiver positions $\boldsymbol{x}_{\boldsymbol{r}i}$, $i = 1, \ldots, 41$, are uniformly distributed on the line $[-5, 5] \times \{0\}$ where both endpoints are receiver positions, that is, the distance between adjacent receivers is 0.25. However, these exact positions are not used to compute the seismograms, instead we place the sources and receivers randomly uniformly distributed in the positive half ball ($x_2 \geq 0$) centered at the respective exact positions with radius 0.1, see Figure 5 (left) for an illustration. The resulting perturbed source/receiver positions are indicated by $\overline{\boldsymbol{x}_{\boldsymbol{s}k}}$ and $\overline{\boldsymbol{x}_{\boldsymbol{r}i}}$, respectively.

So we compute the wave fields

$$u_{i,k}(t) := u(t; \overline{\boldsymbol{x}_{\boldsymbol{r}i}}, \overline{\boldsymbol{x}_{\boldsymbol{s}k}}) \text{ and } \widetilde{u}_{i,k}(t) := \widetilde{u}(t; \overline{\boldsymbol{x}_{\boldsymbol{r}i}}, \overline{\boldsymbol{x}_{\boldsymbol{s}k}}), \quad k \in \{1,2,3\},\ i = 1, \ldots, 41, \tag{44}$$

where t is uniformly sampled in $[0, 30]$ with a sampling rate $\delta\mathrm{t} = 30/m$ for an $m \in \mathbb{N}$ that is set by the wave solver to satisfy the CFL condition. Then, approximating the integral on the right-hand side of (3) by the trapezoidal sum yields 3 seismograms $g_k \in \mathbb{R}^{m \times 41}$, $k = 1, 2, 3$,

$$(g_k)_{j,i} = 4\pi\, \delta\mathrm{t} \Big(\frac{u_{i,k}(j\delta\mathrm{t}) - \widetilde{u}_{i,k}(j\delta\mathrm{t})}{2} + \sum_{\ell=1}^{j-1} \big(u_{i,k}(\ell\delta\mathrm{t}) - \widetilde{u}_{i,k}(\ell\delta\mathrm{t}) \big) \Big). \tag{45}$$

Finally, we add random noise to the seismograms

$$g_k^\varepsilon = g_k + \varepsilon\, \|g_k\|_\star \frac{\mathrm{N}_k}{\|\mathrm{N}_k\|_\star}, \qquad \varepsilon > 0, \tag{46}$$

where N_k is an $m \times 41$ array containing uniformly distributed random numbers in $[-1, 1]$ and ε is the relative noise level with respect to the Frobenius norm $\|\cdot\|_\star$. The seismogram g_3^ε is displayed on the right of Figure 5.

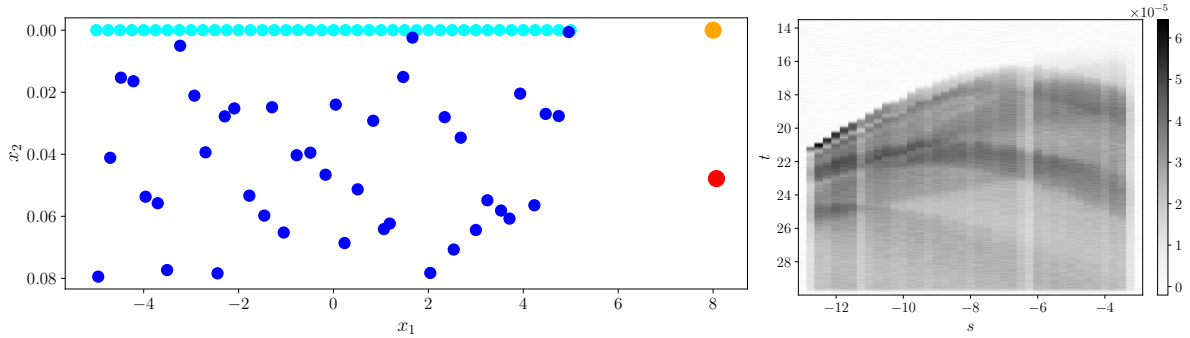

FIGURE 5. Left: Scanning geometry for the source located at $\boldsymbol{x}_{\boldsymbol{s}3} = (8,0)^\top$. The cyan spheres at $x_2 = 0$ show the exact receiver positions, and the blue spheres under them the randomly perturbed receiver positions. Similarly, the orange and the red bullet show the exact and the randomly perturbed positions of the source, respectively. Note the extremely different scalings of the coordinate axes. Right: Corresponding seismogram g_3^ε according to (45) and (46). The receiver positions are parameterized by $\boldsymbol{x}_{\boldsymbol{r}}(s) = (s+8,0)^\top$. The vertical stripes are caused by adjacent receivers having a large vertical distance. Thus, the reflected waves measured at these receivers have significant differences in their amplitudes.

To each source we associate the GRT F_k as in (4) and (5) where we use the common source parametrization $\boldsymbol{x}_{\boldsymbol{s}}(s) = \boldsymbol{x}_{\boldsymbol{s}k}$ and $\boldsymbol{x}_{\boldsymbol{r}}(s) = \boldsymbol{x}_{\boldsymbol{s}k} + (s,0)^\top$ for $s \in \mathcal{S}$. Consequently, the imaging operators $\Lambda^{(i)}$ and $\mathrm{I}_{\mathrm{K}}^{(i)}$, $i = 1,2$, see Sections 3.2 and 3.3, respectively, are defined for each F_k. We have implemented their numerical realizations $L_{k,\gamma}^{(i)}$ and $J_{k,\gamma}^{(i)}$ accordingly, based on the exact source and receiver positions. By setting

$$\mathbb{L}_\gamma^{(i)} := \begin{pmatrix} L_{1,\gamma}^{(i)} & L_{2,\gamma}^{(i)} & L_{3,\gamma}^{(i)} \end{pmatrix} \quad \text{and} \quad \mathbb{J}_\gamma^{(i)} := \begin{pmatrix} J_{1,\gamma}^{(i)} & J_{2,\gamma}^{(i)} & J_{3,\gamma}^{(i)} \end{pmatrix}$$

we get the respective imaging operators for the compound operator $\mathbb{F} = \begin{pmatrix} F_1 & F_2 & F_3 \end{pmatrix}^\top$.

The reconstructions

$$\mathbb{L}_\gamma^{(2)} \begin{pmatrix} g_1^\varepsilon \\ g_2^\varepsilon \\ g_3^\varepsilon \end{pmatrix} = \sum_{k=1}^{3} L_{k,\gamma}^{(2)} g_k^\varepsilon \quad \text{and} \quad \mathbb{J}_\gamma^{(1)} \begin{pmatrix} g_1^\varepsilon \\ g_2^\varepsilon \\ g_3^\varepsilon \end{pmatrix} = \sum_{k=1}^{3} J_{k,\gamma}^{(1)} g_k^\varepsilon$$

are shown for $\gamma = 0.2$ on the left of Figure 6 and, for comparison, on the right we provide $\mathbb{L}_\gamma^{(2)} \left(\begin{smallmatrix} g_1 \\ g_2 \\ g_3 \end{smallmatrix}\right)$ and $\mathbb{J}_\gamma^{(1)} \left(\begin{smallmatrix} g_1 \\ g_2 \\ g_3 \end{smallmatrix}\right)$ with seismograms computed from exact source/receiver positions and without noise, that is, $\varepsilon = 0$. Comparing the right with the left column of Figure 6, we observe that our numerical realizations of the imaging operators are quite robust under the applied perturbations.

We note that there are uniqueness theorems for this data, such as in [21, Chapter I].

6. A GLIMPSE ON THE THREE-DIMENSIONAL SITUATION

Here we consider wave propagation modeled by an analogue of (1) in $\mathbb{R}^3$ and the corresponding linearized inverse problem based on the ansatz (2). Source and receivers are located at $\partial\mathbb{R}^3_+ = \mathbb{R}^2 \times \{0\}$ with positions parametrized by $\boldsymbol{s} = (s_1, s_2)$ in an open subset $S \subset \mathbb{R}^2$. So, the positive x_3-direction points down into the earth or the sea. The three-dimensional versions

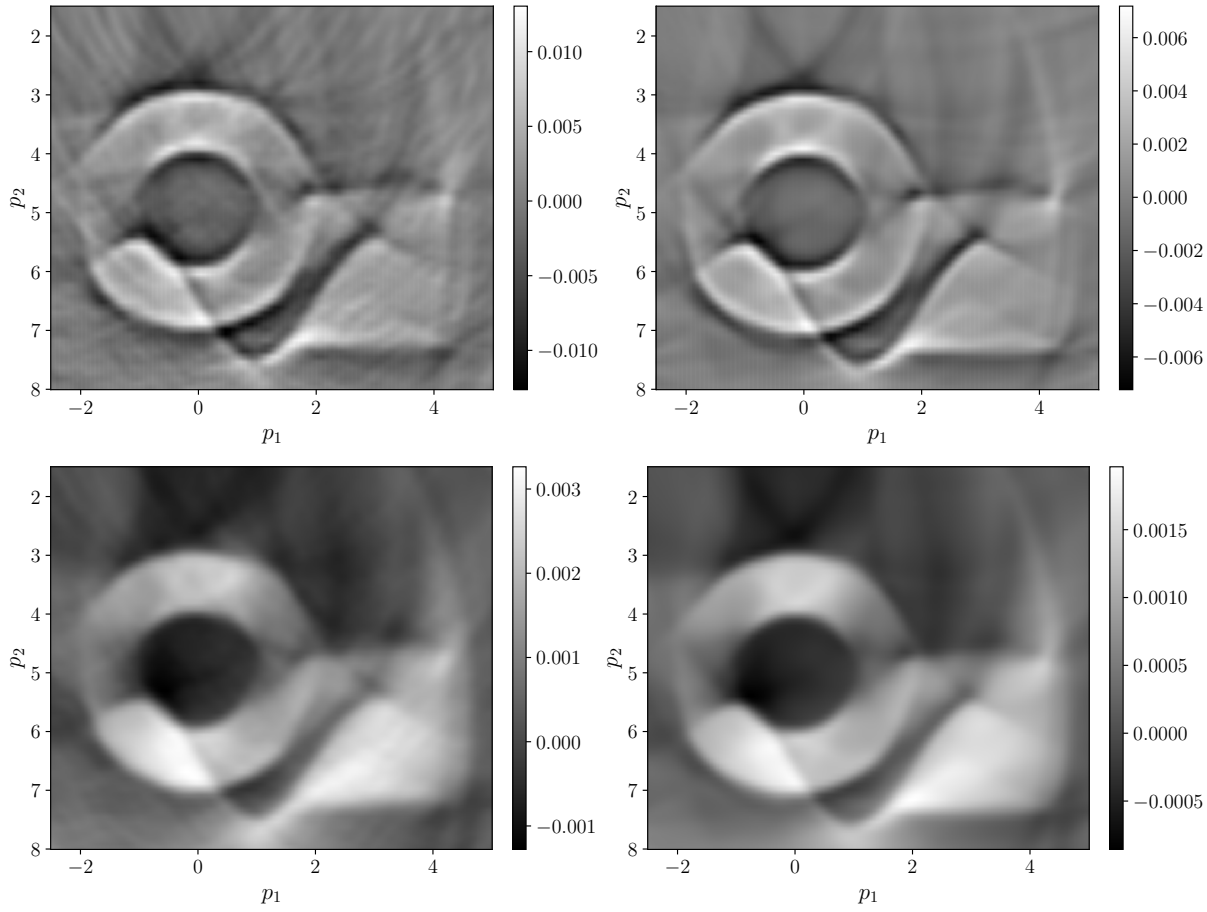

FIGURE 6. Reconstructions of n (Figure 1 top) from common source scanning geometry with the 3 source positions from (43) and 41 receivers. Left: $\mathbb{L}^{(2)}_{0.2}(g_1^\varepsilon\ g_2^\varepsilon\ g_3^\varepsilon)^\top$ (top) and $\mathbb{J}^{(1)}_{0.2}(g_1^\varepsilon\ g_2^\varepsilon\ g_3^\varepsilon)^\top$ (bottom) for the relative noise level $\varepsilon = 5\%$. Right: $\mathbb{L}^{(2)}_{0.2}(g_1\ g_2\ g_3)^\top$ (top) and $\mathbb{J}^{(1)}_{0.2}(g_1\ g_2\ g_3)^\top$ (bottom) where $\varepsilon = 0$ and the wave fields (44) for computing the g_k's (45) have been evaluated at the exact source and receiver positions.

of F and $F_W^\dagger$ are given by the three-dimensional versions of $A = A(\boldsymbol{s}, \boldsymbol{x})$ and $\varphi = \varphi(\boldsymbol{s}, \boldsymbol{x})$. For brevity, we skip some details in this section.

In this three-dimensional setting, the authors of [2] derive the following Kirchhoff operators

$$\mathrm{I}_{\mathrm{K}}^{(1)} = \frac{1}{4\pi^2} F^\dagger_{|B|/A}(\mathrm{Id} \otimes \partial^2)\psi F \quad \text{and} \quad \mathrm{I}_{\mathrm{K}}^{(2)} = \frac{1}{4\pi^2} F^\dagger_{|B|/(v^2 A|\nabla_{\boldsymbol{x}}\varphi|)}(\mathrm{Id} \otimes \partial^3)\psi F$$

where

$$B(\boldsymbol{s}, \boldsymbol{x}) = \det \begin{pmatrix} \nabla_{\boldsymbol{x}}\varphi(\boldsymbol{s}, \boldsymbol{x}) \\ \partial_{s_1}\nabla_{\boldsymbol{x}}\varphi(\boldsymbol{s}, \boldsymbol{x}) \\ \partial_{s_2}\nabla_{\boldsymbol{x}}\varphi(\boldsymbol{s}, \boldsymbol{x}) \end{pmatrix},$$

see [2, (5.1.19) and (5.1.21)]. Their respective orders are 0 and 1.

Our analysis in [9] suggest to define the 3D versions of the filtered normal operators, for instance, by

$$\Lambda^{(1)} = \frac{1}{4\pi^2}(-\Delta)F^\dagger_{|B|/(A|\nabla_{\boldsymbol{x}}\varphi|^2)}\psi F \quad \text{and} \quad \Lambda^{(2)} = \frac{1}{4\pi^2}\partial_{x_3}(-\Delta)F^\dagger_{|B|/(A|\nabla_{\boldsymbol{x}}\varphi|^2)}\psi F$$

having also orders 0 and 1, respectively. For $v(\cdot) = b > 0$ and the zero-offset scanning geometry, $\boldsymbol{x_s}(\boldsymbol{s}) = \boldsymbol{x_r}(\boldsymbol{s}) = (s_1, s_s, 0)^\top$, their symbols, for $\xi_3 \neq 0$, are given by

$$\sigma(\Lambda^{(1)})(\boldsymbol{x},\xi) = \psi\Big(x_1 - \frac{\xi_1}{\xi_3}x_3,\; x_2 - \frac{\xi_2}{\xi_3}x_3\Big) \;\text{ and }\; \sigma(\Lambda^{(2)})(\boldsymbol{x},\xi) = -\imath\xi_3\,\sigma(\Lambda^{(1)})(\boldsymbol{x},\xi)$$

where we used a three-dimensional analogue of Theorem 3.2 and Corollary 3.11 of [9]. Consequently, the statements of Corollary 3.6 carry over yielding

$$\Lambda^{(1)}u = u + O^{(1)}u \quad \text{and} \quad \Lambda^{(2)}u = \partial_{x_3}u + O^{(2)}u$$

with similar restrictions on ψ and u. For those u, $O^{(1)}u$ is one degree smoother in Sobolev scale than u and $O^{(2)}u$ is one degree smoother in Sobolev scale than $\partial_{x_3}u$. Also a 3D adaption of Corollary 3.8 holds for $\mathrm{I}_{\mathrm{K}}^{(1)}$. Beylkin's imaging operator I_{B}, see (36), $\mathrm{I}_{\mathrm{K}}^{(1)}$, and $\Lambda^{(1)}$ are therefore expected to deliver comparable reconstructions in 3D.

Acknowledgments: The authors thank Venky Krishnan for important discussions related to the definition of general ΨDO, (Definition 2.10.)

Todd Quinto and Andreas Rieder are indebted to Alfred K. Louis for his beautiful mathematics, generous mentorship, and warm friendship over the decades.

APPENDIX A. AN AUXILIARY CALCULATION

Set $e = e_1$, see (37). Here, we compute $(-\Delta)^{1/2}e$. Then, $(-\Delta)^{1/2}e_\gamma(\cdot) = (-\Delta)^{1/2}e(\cdot/\gamma)/\gamma^3$. Since

$$(-\Delta)^{1/2}e(\boldsymbol{x}) = \frac{1}{2\pi}\int_{\mathbb{R}^2} |\zeta|\,\widehat{e}(\zeta)\,\mathrm{e}^{\imath\,\boldsymbol{x}^\top\zeta}\,\mathrm{d}\zeta$$

we need

$$\widehat{e}(\zeta) = \frac{2^k\,(k+1)!}{\pi}\,|\zeta|^{-(k+1)}\,\mathrm{J}_{k+1}(|\zeta|)$$

where

$$\mathrm{J}_\nu(z) = \Big(\frac{z}{2}\Big)^\nu \sum_{j=0}^{\infty} \frac{(-1)^j}{j!\,\Gamma(\nu+j+1)}\,\Big(\frac{z}{2}\Big)^{2j}$$

is the *Bessel function of the first kind of order* ν with Γ denoting *Euler's Gamma function*. The expression for $\widehat{e}$ was computed in [20, Example 3.2]. Writing $\boldsymbol{x} = |\boldsymbol{x}|\arg(\boldsymbol{x})$ with $\arg(\boldsymbol{x}) \in S^1$ and using polar coordinates, we get

$$\begin{aligned}(-\Delta)^{1/2}e(\boldsymbol{x}) &= \frac{1}{2\pi}\,\frac{2^k\,(k+1)!}{\pi}\int_{S^1}\int_0^\infty \rho^{1-k}\,\mathrm{J}_{k+1}(\rho)\,\mathrm{e}^{\imath\,\rho|\boldsymbol{x}|\arg(\boldsymbol{x})^\top\Theta}\,\mathrm{d}\rho\,\mathrm{d}\Theta\\ &= \frac{2^k\,(k+1)!}{\pi}\int_0^\infty \rho^{1-k}\,\mathrm{J}_{k+1}(\rho)\,\mathrm{J}_0(|\boldsymbol{x}|\,\rho)\,\mathrm{d}\rho\end{aligned}$$

where, for the last equality, we used the well-known relation

$$\mathrm{J}_0(|\boldsymbol{x}|\rho) = \frac{1}{2\pi}\int_{S^1}\mathrm{e}^{\imath\,\rho|\boldsymbol{x}|\arg(\boldsymbol{x})^\top\Theta}\,\mathrm{d}\Theta.$$

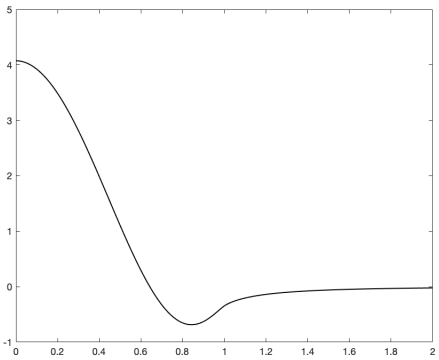

FIGURE 7. Radial part of $(-\Delta)^{1/2}e$ for $e = e_1$, see (37), with $k = 3$.

So we have expressed $(-\Delta)^{1/2}e$ as a generalized Weber-Schafheitlin integral whose value is given in terms of the hypergeometric function ${}_2\mathrm{F}_1$ by

$$(-\Delta)^{1/2}e(\boldsymbol{x}) = \begin{cases} \dfrac{1}{\pi}\dfrac{4^k(k+1)!k!}{(2k)!}\,{}_2\mathrm{F}_1(3/2, 1/2-k; 1; |\boldsymbol{x}|^2) & : |\boldsymbol{x}| \le 1, \\ -\dfrac{1}{2\pi}\,{}_2\mathrm{F}_1(3/2, 3/2; k+2; 1/|\boldsymbol{x}|^2)/|\boldsymbol{x}|^3 & : |\boldsymbol{x}| > 1, \end{cases}$$

see [24] or [7, (6.574)]. The radial part of $(-\Delta)^{1/2}e$ for $k = 3$ is displayed in Figure 7.

REFERENCES

[1] G. BEYLKIN, *Imaging of discontinuities in the inverse scattering problem by inversion of a causal generalized Radon transform*, J. Math. Phys., 26 (1985), pp. 99–108, http://dx.doi.org/10.1063/1.526755.

[2] N. BLEISTEIN, J. K. COHEN, AND J. W. STOCKWELL, JR., *Mathematics of multidimensional seismic imaging, migration, and inversion*, vol. 13 of Interdisciplinary Applied Mathematics, Springer-Verlag, New York, 2001, http://dx.doi.org/10.1007/978-1-4613-0001-4. Geophysics and Planetary Sciences.

[3] L. DEMANET AND R. J. HEWETT, PySIT – *Seismic Imaging Toolbox for Python* v1.0. http://pysit.org.

[4] R. FELEA, V. P. KRISHNAN, C. J. NOLAN, AND E. T. QUINTO, *Common midpoint versus common offset acquisition geometry in seismic imaging*, Inverse Probl. Imaging, 10 (2016), pp. 87–102, https://doi.org/10.3934/ipi.2016.10.87.

[5] K. GANSTER, *A microlocal and visual comparison of 2D Kirchhoff migration formulas - software package*, 2024, https://dx.doi.org/10.35097/YeHLCWQEafknUBDA.

[6] K. GANSTER AND A. RIEDER, *Approximate Inversion of a Class of Generalized Radon Transforms*, SIAM J. Imaging Sci., 16 (2023), pp. 842–866, https://doi.org/10.1137/22M1512417.

[7] I. S. GRADSHTEYN AND I. M. RYZHIK, *Table of integrals, series, and products*, Academic Press [Harcourt Brace Jovanovich, Publishers], New York-London-Toronto, 1980.

[8] C. GRATHWOHL, P. KUNSTMANN, E. T. QUINTO, AND A. RIEDER, *Microlocal analysis of imaging operators for effective common offset seismic reconstruction*, Inverse Problems, 34 (2018), pp. 114001, 24, https://doi.org/10.1088/1361-6420/aadc2a.

[9] C. GRATHWOHL, P. KUNSTMANN, E. T. QUINTO, AND A. RIEDER, *Imaging with the elliptic Radon transform in three dimensions from an analytical and numerical perspective*, SIAM J. Imaging Sci., 13 (2020), pp. 2250–2280, https://doi.org/10.1137/20M1332657.

[10] V. GUILLEMIN, *On some results of Gel'fand in integral geometry*, in Pseudodifferential operators and applications (Notre Dame, Ind., 1984), vol. 43 of Proc. Sympos. Pure Math., Amer. Math. Soc., Providence, RI, 1985, pp. 149–155, https://doi.org/10.1090/pspum/043/812288.

[11] V. GUILLEMIN AND S. STERNBERG, *Geometric asymptotics*, American Mathematical Society, Providence, R.I., 1977. Mathematical Surveys, No. 14.
[12] S. HELGASON, *Integral geometry and Radon transforms*, Springer, New York, 2011, http://dx.doi.org/10.1007/978-1-4419-6055-9.
[13] L. HÖRMANDER, *Fourier integral operators. I*, Acta Math., 127 (1971), pp. 79–183, http://link.springer.com/article/10.1007/BF02392052.
[14] L. HÖRMANDER, *The analysis of linear partial differential operators. I*, Classics in Mathematics, Springer-Verlag, Berlin, 2003. Distribution theory and Fourier analysis, Reprint of the second (1990) edition [Springer, Berlin].
[15] V. P. KRISHNAN AND E. T. QUINTO, *Microlocal analysis in tomography*, in Handbook of Mathematical Methods in Imaging, O. Scherzer, ed., Springer Reference, Springer, 2015, pp. 847–902, http://dx.doi.org/10.1007/978-1-4939-0790-8_36.
[16] P. C. KUNSTMANN, E. T. QUINTO, AND A. RIEDER, *Seismic imaging with generalized Radon transforms: stability of the Bolker condition*, Pure Appl. Math. Q., 19 (2023), p. 1985–2036, https://dx.doi.org/10.4310/PAMQ.2023.v19.n4.a11.
[17] A. K. LOUIS, *"Approximate inverse for linear and some nonlinear problems" [Inverse Problems* **11** *(1995), no. 6, 1211–1223]*, Corrigendum: Inverse Problems, 12 (1996), pp. 175–190, http://dx.doi.org/10.1088/0266-5611/12/2/005.
[18] B. E. PETERSEN, *Introduction to the Fourier transform and pseudo-differential operators*, vol. 19 of Monographs and Studies in Mathematics, Pitman (Advanced Publishing Program), Boston, MA, 1983.
[19] E. T. QUINTO, *The dependence of the generalized Radon transform on defining measures*, Trans. Amer. Math. Soc., 257 (1980), pp. 331–346, https://doi.org/10.2307/1998299.
[20] A. RIEDER, *Principles of reconstruction filter design in 2D-computerized tomography*, in Radon transforms and tomography (South Hadley, MA, 2000), vol. 278 of Contemp. Math., Amer. Math. Soc., Providence, RI, 2001, pp. 207–226, http://dx.doi.org/10.1090/conm/278/04606.
[21] V. G. ROMANOV, *Integral Geometry and Inverse Problems for Hyperbolic Equations*, vol. 25 of Springer tracts in Natural Philosophy, Springer-Verlag, New York, Heidelberg, Berlin, 1974.
[22] W. RUDIN, *Functional analysis*, McGraw-Hill Book Co., New York-Düsseldorf-Johannesburg, 1973. McGraw-Hill Series in Higher Mathematics.
[23] T. SCHUSTER, *The method of approximate inverse: theory and applications*, vol. 1906 of Lecture Notes in Mathematics, Springer, Berlin, 2007, http://dx.doi.org/10.1007/978-3-540-71227-5.
[24] H. M. SRIVASTAVA AND H. EXTON, *A generalization of the Weber-Schafheitlin integral*, J. Reine Angew. Math., 309 (1979), pp. 1–6, https://doi.org/10.1515/crll.1979.309.1.
[25] W. W. SYMES, *Mathematics of reflection seismology*, tech. report, The Rice Inversion Project, Rice University, Houston, TX, USA, 1998, http://www.trip.caam.rice.edu/downloads/preamble.pdf.
[26] F. TRÈVES, *Introduction to pseudodifferential and Fourier integral operators. Vol. 1*, Plenum Press, New York-London, 1980. Pseudodifferential operators, The University Series in Mathematics.
[27] F. TRÈVES, *Introduction to pseudodifferential and Fourier integral operators. Vol. 2*, Plenum Press, New York-London, 1980. Fourier integral operators, The University Series in Mathematics.

DEPARTMENT OF MATHEMATICS, KARLSRUHE INSTITUTE OF TECHNOLOGY (KIT), D-76128 KARLSRUHE, GERMANY
Email address: kevin.ganster@kit.edu
Email address: andreas.rieder@kit.edu

DEPARTMENT OF MATHEMATICS, TUFTS UNIVERSITY, MEDFORD, MA 02155, USA
Email address: todd.quinto@tufts.edu